ISTANBUL TECHNICAL UNIVERSITY ★ GRADUATE SCHOOL

INTERACTION BETWEEN MAGNETIZED STARS AND DISKS

Ph.D. THESIS

Murat Metehan TÜRKOĞLU

Department of Physics Engineering

Physics Engineering Programme

NOVEMBER 2021

ISTANBUL TECHNICAL UNIVERSITY ★ GRADUATE SCHOOL

INTERACTION BETWEEN MAGNETIZED STARS AND DISKS

Ph.D. THESIS

Murat Metehan TÜRKOĞLU
(509102122)

Department of Physics Engineering

Physics Engineering Programme

Thesis Advisor: Prof. Dr. Kazım Yavuz EKŞİ

NOVEMBER 2021

İSTANBUL TEKNİK ÜNİVERSİTESİ ★ LİSANSÜSTÜ EĞİTİM ENSTİTÜSÜ

MANYETİK YILDIZLAR VE DİSKLER ARASINDAKİ ETKİLEŞİM

DOKTORA TEZİ

Murat Metehan TÜRKOĞLU
(509102122)

Fizik Mühendisliği Anabilim Dalı

Fizik Mühendisliği Programı

Tez Danışmanı: Prof. Dr. Kazım Yavuz EKŞİ

KASIM 2021

Murat Metehan TÜRKOĞLU, a Ph.D. student of ITU Graduate School with ID number 509102122, successfully defended the thesis entitled "INTERACTION BETWEEN MAGNETIZED STARS AND DISKS", which he prepared after fulfilling the requirements specified in the associated legislations, before the jury whose signatures are below.

Thesis Advisor :	**Prof. Dr. Kazım Yavuz EKŞİ** Istanbul Technical University	.....
Jury Members :	**Prof. Dr. Kazım Yavuz EKŞİ** Istanbul Technical University	.....
	Assoc. Prof. Abdurrahman Savaş ARAPOĞLU Istanbul Technical University	.....
	Prof. Dr. Tolga GÜVER Istanbul University	.....
	Assoc. Prof. Tolga BİRKANDAN Istanbul Technical University	.....
	Prof. Dr. Ahmet Togo GİZ MEF University	.....

Date of Submission : 15 November 2021
Date of Defense : 30 November 2021

To my wife, Eda Armağan TÜRKOĞLU, To my mom, Refiye DEROGEÇ and my family,

FOREWORD

First and foremost this thesis could never have been completed without patience and support of my wife, Eda Armağan TÜRKOĞLU and my mother, Refiye DEROGEÇ.

I also would like to thank my Ph.D. advisor, Kazım Yavuz EKŞİ for introducing me to astrophysics and for sharing his knowledge and support.

Finally, I am obligated to Scientific and Technological Research Council of Turkey (TUBITAK) for supporting me as Ph.D. student scholar with the project number of 112T105.

November 2021

Murat Metehan TÜRKOĞLU
(Ph.D.)

TABLE OF CONTENTS

Page

ABBREVIATIONS

ADAF : Accretion Dominated Accretion Flow
BFM : Beat Frequency Model
AMXP : Accreting Millisecond X-ray Pulsar
HMXB : High-mass X-ray binary
BH : Black Hole
BLM : Boundary Layer Model
CCO : Central Compact Object
CVs : Cataclysmic Variables
DIM : Disk Instability Model
IMBH : Intermediate Mass Black Hole
LMXB : Low-mass X-ray binary
MRI : Magneto-Rotational Instability
MSP : Millisecond Pulsar
MTD : Magnetically Threaded Disk Model
NASA : National Aeronautics and Space Administration
NS : Neutron Star
QPO : Quasi Periodic Oscillation
PCU : Proportional Counter Unit
RPP : Rotation Powered Pulsar
WD : White Dwarf
ULX : ultraluminous X-ray Source

SYMBOLS

$\mathbf{b}$	:	Beaming factor
$\mathbf{B}$	:	Magnetic field
$\mathbf{B_z}$	:	Poloidal magnetic field of neutron star
$\mathbf{B_\phi}$	:	Toroidal magnetic field of neutron star
$\mathbf{c}$	:	Light speed
$\mathbf{C_s}$	:	Sound speed
$\mathbf{d}$	:	Distance of the star
δ	:	Relative width of boundary region
ε	:	Efficiency of gravitational energy release
$\phi_{\mathbf{R}}(\mathbf{r})$	:	Critical Potential
$\mathbf{F}$	:	Flux; Force
$\mathbf{F_c}$	:	Critical flux
γ_ϕ	:	Azimuthal pitch
$\mathbf{G}$	:	Gravitational constant
$\mathbf{H}$	:	Scale-height
$\mathbf{L}$	:	Luminosity; Lagrange point
$\mathbf{m_p}$	:	Mass of proton
$\mathbf{M_*}$	:	Mass of the compact star
$\mathbf{M_d}$	:	Mass of the donor star
$\mathbf{M_\odot}$	:	Solar mass
μ	:	Magnetic dipole moment
$\dot{\mathbf{M}}$	:	Accretion rate
$\mathbf{n}(\omega)$	:	dimensionless torque
$\mathbf{N_{disk}}$	:	The torque applied by the disk
$\nu_\mathbf{K}$	:	Keplerian frequency
$\nu_\mathbf{s}$	:	Spin frequency
$\mathbf{P}$	:	Period of the star
$\mathbf{P_{orb}}$	:	Orbital period
$\mathbf{N_*}$	:	The torque applied to the star
ω_*	:	Fastness parameter
Ω_K	:	Keplerian angular velocity
ω_orb	:	Orbital angular velocity
$\Omega_\mathrm{K}(\mathbf{R_m})$	:	Keplerian angular velocity at the inner radius
$\mathbf{P_c}$	:	Critical period
$\mathbf{R_*}$	:	Radius of the star
$\mathbf{R_A}$	:	Alfvén radius
$\mathbf{R_c}$	:	Corotation radius
$\mathbf{R_{ISCO}}$	:	Innermost stable circular orbit
$\mathbf{R_{in}}$	:	Inner radius of the disk
$\mathbf{R_L}$	:	Radius of the light cylinder
$\mathbf{R_m}$	:	Magnetospheric radius
$\mathbf{R_{sp}}$	:	Spherization radius
$\sigma_\mathbf{T}$	:	Thomson cross-section

LIST OF TABLES

Page

LIST OF FIGURES

Page

INTERACTION BETWEEN MAGNETIZED STARS AND DISKS

SUMMARY

X-ray binary systems consist of a compact object, such as a neutron star, white dwarf or black hole, and a normal star that transfers mass to this compact object. X-ray binary systems are split into two groups depending on the mass of the donor star. If the mass of the donor star is $M_d \leq 1M_\odot$, these kinds of systems are called LMXB and if the donor star mass is $M_d > 10M_\odot$, these systems are known as HMXB. The other component of the X-ray binary systems are compact stars: white dwarfs, neutron stars or black holes. The observed X-ray power of these systems originate from the gravitational potential energy released by the accretion of matter onto the compact star and depends on the compactness, M_*/R.

In LMXB, matter from the outer envelope of the donor star may may be transferred to the compact star by Roche lobe overflow. In HMXB, matter from the outer envelope of the donor star may be transferred to compact star by stellar wind. In both cases because the matter transferred from the donor star has angular momentum, the matter can not accrete on to the compact object directly; instead an accretion disk forms. The physical parameters that define the interaction between a neutron star and a surrounding disk are the magnetic field and angular velocity of the of the compact star, and the mass flow rate in the disk. The interactions occur in three different stages:

i-) *Mass accretion stage:* If the inner radius of the disk, $R_{\rm m}$, is smaller than the corotation radius, $R_{\rm co}$, the matter follows the magnetic field lines and flow to the polar caps of the neutron stars.

ii-) *Propeller stage:* In this stage, $R_{\rm m} > R_{\rm co}$, the matter at the inner region of the disk meets with more rapidly rotating field lines attached to the star. A decline may occur in the observed X-ray flux because the mass accretion is centrifugally inhibited.

iii-) *Radio pulsar stage:* If the inner radius of the disk is larger than the light cylinder radius, $R_{\rm L}$, an interaction can not occur between the neutron star and the disk. In this stage, the cause of the observed X-ray flux is the slowing down of the rotation of the neutron star.

The QPO are thought to be generated in regions close to the neutron star and the inner part of the disk. Therefore, special types of QPOs provide direct evidence for disk-magnetosphere interaction. In this study, models were created by using both observational physical parameters (period, period derivative, luminosity, etc) and QPOs.

The observation that the X-ray luminosity does not change significantly during transitions to the spin-down stage led to MTD of Ghosh & Lamb in 1979. In

this model, magnetic field can thread the disk by instabilities between disk and magnetosphere and the presence of turbulence in the disk. The magnetic field lines slip around the disk due to the differential rotation between disk and the neutron star. According to the Ghosh & Lamb model, there is a stable region in which the twisted magnetic field balances the spread magnetic field around the disk. In this way a toroidal magnetic field is generated. However, as long as the magnetic field gets twisted around the disk, arbitrarily strong toroidal magnetic field is generated and such strong magnetic fields can destroy the disk. Because of the problems mentioned above, Ghosh & Lamb model have important inadequacies.

The magnetic field lines that penetrate the disk beyond the corotation radius slow down the neutron star. The net torque acting on the neutron star is the sum of the material torque which spins up the star and the magnetic torque which slows down the star. Toroidal magnetic field is an important factor that determines the net torque. In order to understand the long-term evolution of the neutron star, it is important to specify how the torque depends on the fastness parameter, ω_*.

As LMXB have weak magnetic fields, it is hard to observe the spin change of the system. Also HMXB have stellar winds that affect the torque and observed luminosity, the relation between the fastness and the torque can not be specified, sensitively. For these reasons, we choose *4U–1626 67* which has high magnetic field and accretes from a low mass donor star. *4U–1626 67* underwent two torque reversals in June 1990 and February 2008. We used the torque reversal data and explored the coherence between observational data and some torque models in the literature.

It is discovered that each nearby galaxy host one or two "*ultraluminous X-ray sources*" (ULXs) whose luminosity exceed the Eddington limit for a solar mass object. It was initially assumed that the ULX host IMBH but later with the discovery of X-ray pulsations from some of these objects (e.g *M82 X-2, ULX NGC 5907, ULX NGC 7793 P-13, NGC 300 ULX1, M51 ULX-7, NGC 1313 X-2 and Swift J0243.6+6124*) showed that they at least some of them are neutron stars. Population studies indicate that the accreting neutron stars are common sources in the ULX population. In this thesis, we investigate the surface magnetic field dipole strength, beaming fraction and fastness parameter of the, PULX, taking into account the accretion flow in the super-critical regime, beaming of X-ray emission and the reduction of the scattering cross section in the presence of a strong magnetic field. We used three different methods for determining the magnetic fields of the PULX:

i-) We assume the system to be near torque equilibrium.

ii-) We rely on the spin-up rate and solve the torque equation.

iii-) We assume the systems to be accreting at the critical rate. This critical rate depends on the electron scattering cross-section determined by the super-critical magnetic fields.

The plan of the thesis is as follows: In Chapter 1, the main ideas of the star-disk interactions are given. In Chapter 2, the flux, the period and the period derivative data of *4U-1626 67* embracing the torque reversal events in June 1990 and February 2008 are analysed and compared with Ghosh-Lamb model and some other models in the literature. In Chapter 3, the magnetic fields of the pulsating X-ray sources are

calculated using three different assumptions. Also, as the beaming fraction depends on the inner radius of the disc which in turn depends on the mass accretion rate, we find that the isotropic-equivalent luminosity of the source does not depend linearly on the mass accretion rate. In Chapter 4 all of the results are discussed.

MANYETİK YILDIZLAR VE DİSKLER ARASINDAKİ ETKİLEŞİM

ÖZET

X-ışın çift yıldız sistemleri, bir nötron yıldızı veya kara delik gibi kompakt bir nesne ve bu kompakt nesnelere kütle aktaran normal bir yıldızdan oluşur. X-ışın çift yıldız sistemleri, donör yıldızın kütlesinin $M_d \leq 1M_\odot$ olduğu düşük kütleli X-ışın sistemleri ve donör yıldızın kütlesinin $M_d \geq 10M_\odot$ olduğu büyük kütleli X-ışın sistemleri olarak ikiye ayrılmaktadır. Bu tür sistemlerde diğer bileşen bir tıkız nesnedir; beyaz cüce, nötron yıldızı ya da karadelik. Gözlenen X-ışınlarının nedeni tıkız nesne üzerine aktarılan maddenin gravitasyonel potansiyel enerjisinin X-ışın akısına dönüşmesidir ve yayılan enerji yıldızın tıkızlığına, M_*/R, bağlıdır.

Düşük kütleli X-ışın sistemlerinde donör yıldızın dış katmanları, Roche lobunu doldurması nedeniyle, tıkız nesne üzerine akabilir. Büyük kütleli X-ışın sistemlerinde ise donör yıldızın dış katmanları yıldız rüzgarları formunda tıkız nesne üzerine aktarılabilir. Donör yıldızdan aktarılan maddenin tıkız yıldıza göre açısal momentuma sahip olması nedeniyle aktarılan madde tıkız nesne üzerine direkt olarak düşmez bunun yerine tıkız nesne etrafında bir disk oluşturur. Disk ile tıkız nesne arasındaki etkileşimi belirleyen faktörler tıkız nesnenin manyetik alanı, dönme hızı ve kütle aktarım oranıdır. Disk-manyetosfer etkileşimi üç farklı evrede gerçekleşir:

i-) *Kütle Aktarım Evresi:* Diskin iç yarıçapı, $R_{\rm m}$, eş dönme yarıçapından, $R_{\rm co}$, küçükse disk manyetik alan çizgilerini takip ederek nötron yıldızının kutup bölgelerine akar.

ii-) *Pervane Evresi:* Diskin iç yarıçapı, $R_{\rm m}$, eş dönme yarıçapından, $R_{\rm co}$, büyükse diskin iç bölgesindeki madde, nötron yıldızının daha hızlı dönmesi nedeniyle bir merkezkaç bariyeri ile karşılaşır. Kutup bölgesine akan madde miktarında azalma olduğundan gözlemlenen X-ışınımında bir düşüş meydana gelir.

iii-) *Radyo Pulsarı Evresi:* Diskin iç yarıçapı ışık silindiri yarıçapından büyükse disk ile nötron yıldızı arasında bir etkileşim gerçekleşmez. Bu evrede görülen X-ışınımının nedeni nötron yıldızının dönme hızının yavaşlamasıdır.

Yarı periyodik salınımların (QPO), nötron yıldızına yakın bölgelerde ve diskin iç kısımlarında üretildiği düşünülmektedir. Bu nedenle özel tipteki salınımlar disk-manyetosfer etkileşimi için doğrudan kanıt sağlamaktadır. Bu çalışmada salınımlar ile birlikte diğer gözlemsel fiziksel parametreler (periot, periot türevi, ışınım vb) kullanılarak modeller oluşturulmuştur.

Bazı nötron yıldızlarını yavaşladıklarının anlaşılması ve yavaşlarken X-ışın parlaklığında önemli bir değişim gözlenmemesi nedeniyle Ghosh & Lamb tarafından 1979 yılında "manyetik olarak nüfuz edilmiş disk" modeli, MTD, öne sürülmüştür. Bu

modelde akışkanlar arasındaki kararsızlıklar ve diskin türbülanslı olması nedeniyle manyetik alan diske nüfuz edebilmektedir. Disk ve yıldız arasındaki diferansiyel dönme nedeniyle manyetik alan çizgileri disk etrafında kayar. Ghosh & Lamb modeline göre manyetik alan çızgilerinin bükülmesi ve disk içinde yayılmasının dengelendiği kararlı bir bölge mevcuttur. Böylece disk toroidal bir manyetik alan oluşturmaktadır. Bununla birlikte manyetik alanın disk etrafında bükülmesinin keyfi büyük manyetik alanlar meydana getirmesi ve oluşan bu manyetik alanların diski parçalama olasılığı Ghosh & Lamb modelininin en önemli yetersizliklerinden biridir.

Eş dönme yarıçapının ötesindeki manyetik alan çizgileri yıldızı yavaşlatırken, eş dönme yarıçapının içinde bulunan manyetik alan çizgileri yıldızı hızlandırmaktadır. Nötron yıldızı üzerine etki eden net tork hızlandırıcı maddesel tork ve yavaşlatıcı manyetik torkun toplamıdır. Toroidal manyetik alanı kısıtlayan mekanizmanın ne olduğu tam olarak anlaşılamamış olsa da, toroidal manyetik alan torku belirleyen önemli faktörlerden biridir. Nötron yıldızının uzun süreli evriminin anlaşılabilmesi için, torkun yıldızın dönme hızına nasıl bağlı olduğunun belirlenmesi gerekir.

Düşük kütleli X-ışın çift sistemleri küçük manyetik alanlara sahip olması nedeniyle spin değişimlerini gözlemlemek güçtür. Bununla birlikte büyük kütleli X-ışın çift sistemleri ölçülen ışınımı ve torku etkileyen yıldız rüzgarlarına sahip olduğundan spin değişimi-tork ilişkisini belirlemek zordur.

Bu tez çalışmasında, yukarıda bahsettiğimiz nedenlerden dolayı, yüksek bir manyetik alana sahip ve düşük kütleli eşlikçisinden kütle aktarımı yapan *4U–1626 67* kaynağı seçilmiş olup, Haziran 1990 ve Şubat 2008'de görülen iki tersine dönen tork değişim verileri kullanılarak literatürdeki tork modellerinin gözlemsel verilerle uyumluluğu araştırılmıştır.

Yakın galaksilerin her birinde parlaklığı Eddington limitini aşan ve kütlesi Güneş kütlesine yakın bir ya da iki "*aşırı parlak X-ışın kaynağı*", (ULX), keşfedilmiştir. Başlangıçta bu tür kaynakların orta kütleli karadelikler olduğu varsayılmış olsa da Bachetti ve diğerleri tarafından 2014 yılında keşfedilen *PULX M82 X-2*, Israel ve diğerleri tarafından 2016 yılında keşfedilen *ULX NGC 5907*, Israel ve diğerleri ve Furst ve diğerleri tarafından yine 2016 yılında keşfedilen *ULX NGC 7793 P13*, Carpano ve diğerleri tarafından 2018 yılında keşfedilen *NGC 300 ULX1*, Rodriguez Castillo ve diğerleri tarafından 2019 yılında keşfedilen *M51 ULX7*, Sathyaprakash ve diğerleri tarafından 2019 yılında keşfedilen *NGC 1313 X2* ve Wilson Hodge ve diğerleri tarafından 2018 yılında keşfedilen *Swift JO243.6+6124* kaynaklarından X-ışın atımları gözlenmesi aşırı parlak X-ışın kaynakları içinde nötron yıldızlarının varlığına dair kanıtlar ortaya koymuştur.

Bu tez çalışmasında, süper-kritik rejimdeki aktarım akışını, X-ışın parlaklığını ve güçlü bir manyetik alanın varlığında foton tesir kesiti saçılımının azalmasını dikkate alarak, kaynakların yüzey manyetik alan dipol şiddetini, hüzmelenme kesrini ve hız parametresini inceledik. PULX'lerin manyetik alanlarının belirlemek için üç farklı yöntem kullandık:

i-) Sistemin neredeyse tork dengesinde olduğunu varsayıyoruz.

ii-) Hızlanma oranına dayanarak tork denklemini çözüyoruz.

iii-) Sistemlerin kritik oranda aktarım yaptığını varsayıyoruz. Bu kritik oran, manyetik alan tarafından belirlenen elektron saçılma tesir kesitine bağlıdır.

Bu tez çalışmasının planı şu şekildedir: 1. bölümde disk-manyetosfer etkileşiminin temel kavramları hakkında bilgiler verilmiştir. 2. bölümde *4U–1626 67* kaynağının Haziran 1990 ve Şubat 2008'de gösterdiği iki tersine dönen torka ait periyot, periyot türevi ve akı verileri interpolasyon yöntemiyle çoğaltılıp elde edilen sonuçlar Ghosh & Lamb modeli ve diğer bazı modellerle karşılaştırılmıştır. 3. bölümde, aşırı parlak kaynakların manyetik alanları, üç farklı varsayım kullanılarak hesaplanmıştır. Ayrıca, hüzmelenme oranı diskin iç yarıçapına bağlı olduğundan, (bu da kütle aktarım hızına bağlıdır) kaynağın izotropik eşdeğer parlaklığının kütle aktarım hızına doğrusal olarak bağlı olmadığı gösterilmiştir. 4. bölümde ise elde edilen tüm sonuçlar ve kullanılan yöntemler özetlenmiştir.

1. INTRODUCTION TO DISK-MAGNETOSPHERE INTERACTION

1.1 Introduction

Interaction between a magnetized star and an accretion disk may occur in various astrophysical objects. For example, the interactions can be observed in the T–Tauri stars [1], in the Cataclysmic Variables (CVs) [2] or in the accretion powered pulsars [3].

Most of the stars in our galaxy are in the binary systems. The star with the larger mass evolves more rapidly and becomes a compact object. During their evolution, the normal star may increase in radius or the binary separation may shrink. This may lead the star to fill its Roche lobe and then its outer envelope may flow onto the compact star (*Roche lobe overflow*). A star with a higher mass ejects its outer envelope in the form a stellar wind. Some of this material may be captured by the compact star (*wind accretion*).

In the accretion process a large amount of radiation is released and thus accretion powered pulsars are much brighter than non-accreting neutron stars. The released energy depends on the *compactness*, M_*/R_*, ratio of mass and radius of the compact star. In order that the disk material can fall onto the compact star, the angular momentum of the disk must be transported outward. The angular momentum of the disk must be transported outward for disk material to fall onto the compact star. Some instabilities, for example magneto-rotational instability (MRI) [4], cause turbulence which causes enhanced turbulent viscosity.

The first studies about effective viscosity in accretion disks were performed by Shakura & Sunyaev [5]. According to Shakura & Sunyaev (1973) theory, the viscosity, ν, depends on the pressure scale height, H, and sound speed, C_s, in the disk; $\nu = \alpha C_s H$ where $\alpha < 1$ is a constant.

1.2 Roche Lobe Overflow

The Roche potential is the potential experienced by a test particle in the gravitational potential of two massive objects (compact star and donor star) orbiting each other. According to the this approximation the orbits are circular.

In addition to the force arising from the two massive objects, the centrifugal and the Coriolis force act on the test particle. But the Coriolis force vanishes if the test particle is at rest in the binary frame. The Roche potential is defined as follows;

$$\phi_R(r) = -\frac{GM_1}{|\overrightarrow{r} - \overrightarrow{r_1}|} - \frac{GM_2}{|\overrightarrow{r} - \overrightarrow{r_2}|} - \frac{1}{2}(\overrightarrow{\omega}_{\text{orb}} \times \overrightarrow{r})^2. \tag{1.1}$$

where G is the gravitational constant, $\overrightarrow{r}$, $\overrightarrow{r}_1$, $\overrightarrow{r}_2$ are the position vectors of the stars, M_1 and M_2 are the masses of the compact star and the donor star and $\overrightarrow{\omega}_{\text{orb}}$ defines the orbital angular frequency. The first two terms of Eq.1.1 defines the gravitational attraction of the stars and the gradient of the third term gives the centrifugal force.

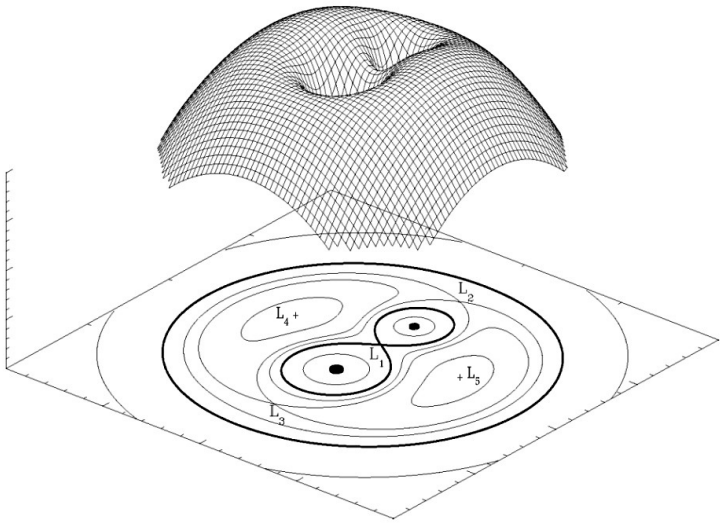

Figure 1.1 : Roche potential of a binary system [6].

The shape of the equivalent potential is determined by the mass ratio, $q = M_2/M_1$, of the objects. The Lagrange points are seen in Figure 1.1 [6]. There are 5 points (so called Lagrange points, L_2, L_3, L_4, L_5) at which the Roche potential is an extremum and hence the net force acting on a test particle is zero. The first Lagrange point L_1 is at the intersection of the two lobes. This means that when the material comes to the L_1 point, the material can pass through into the other lobe, easily. When the donor star fills its Roche lobe, the material of the donor star is transferred from the L_1 point. Since the material has angular momentum, the accreting material can not fall on to the compact object directly but an accretion disk forms.

The X-ray binary systems are divided into two main categories with several subclasses. In low-mass X-ray binaries (LMXB), mass of the companion star is approximately $M_d \lesssim 1\ M_\odot$ where $M_\odot$ is the mass of the sun, and the mass transfer usually occurs by Roche lobe overflow. In high mass X-ray binaries (HMXBs) the mass of the companion star is $M_d \gtrsim 10\ M_\odot$ mass transfer occurs via stellar wind.

1.3 The Basics Concepts of Disk-Magnetosphere Interaction

In X-ray pulsars, the matter inflowing in the disk is channeled from the inner region of the disk to the magnetic poles of a neutron star. The magnetic field is not aligned with the rotation axis and if the hot polar cap, in each rotation of the star, passes from our line of sight, we observe an X-ray pulse.

The magnetic field of the star disrupts the flow at a distance larger than the radius of the star. In spherical mass accretion the magnetospheric radius where the magnetic pressure is balanced with the ram pressure is the Alfvén radius,

$$R_{\rm A} = \left(\frac{\mu^4}{2GM_*\dot{M}^2}\right)^{1/7} \tag{1.2}$$

where μ is the magnetic moment of the magnetized star and $\dot{M}$ is the mass accretion rate [7].

In the case of disk accretion, the inner radius of the disk scales with the Alfvén radius so that $R_{\rm m} = \zeta R_{\rm A}$ where $R_{\rm m}$ is the magnetospheric radius and ζ a dimensionless constant of order unity; according to the Ghosh & Lamb model [8] ζ is 0.52.

The corotation radius where the Keplerian rotation rate in the disk is equal to the rotation rate of the star, is written as;

$$R_{\rm c} = \left(\frac{GM_*P^2}{4\pi^2}\right)^{1/3}. \tag{1.3}$$

where $R_{\rm c}$ is the corotation radius and P is the period of the star. Another characteristic length for neutron stars is the light cylinder radius. The light cylinder radius distinguishes the inner domain of the magnetosphere which has static magnetic field different from the outer radiation zone, and is defined as;

$$R_{\rm L} = \frac{c}{\Omega_*}. \tag{1.4}$$

where c is the speed of light and Ω_* is the angular velocity of the star. The rotation parameter of the system, ω_*, called the fastness parameter, is defined as;

$$\omega_* = \frac{\Omega_*}{\Omega_K(R_{\rm m})}. \tag{1.5}$$

where $\Omega_K(R_{\rm m})$ is the Keplerian angular velocity at the inner radius. Neutron stars can interact with their surrounding disks in three different modes depending on the size of the magnetosphere with respect to two different characteristic radii, the corotation radius and the light cylinder radius: *(i)* Mass accretion mode $(R_{\rm m} < R_{co}, \omega_* < 1)$; *(ii)* Propeller mode $(R_{\rm L} > R_{\rm m} > R_{\rm co}, \omega_* > 1)$; *(iii)* Radio pulsar mode $(R_{\rm m} > R_{\rm L})$.

In the accretion mode the gravitational potential energy of the falling matter on to the star is converted to heat and radiation. Total luminosity coming from the stellar surface is;

$$L = \frac{GM_*\dot{M}}{R_*} \tag{1.6}$$

where M_* and R_* are the mass and the radius of the star, respectively. If the outward pressure of radiation exceeds the inward gravitational accretion, then accretion can be halted. This limit is known as the Eddington limit given by;

$$L_{Edd} = \frac{4\pi GMcm_p}{\sigma_T}. \tag{1.7}$$

where m_p is the mass of the proton and σ_T is the Thompson cross section [9].

According to Eq. 1.2, the inner radius of the disk will become smaller with the mass accretion rate. If the mass accretion rate decreases sufficiently enough, the inner radius of the disk goes beyond the corotation radius and the system enters the propeller regime. In the propeller regime, it is expected that the matter carried to the inner edge of the disk does not fall onto the surface of the star because of the centrifugal barrier [10], but is ejected out of the system. The assumption that the matter can not fall onto the neutron star in the propeller regime is valid only if the thickness of the disk is infinitely thin and the magnetic axis coincides with spin axis. In reality, some fraction of the inflowing matter might fall onto the star even when $\omega_* > 1$ (see e.g [11]). Also, the description of the magnetospheric radius given by Eq. 1.2 only prevails in the case of steady state. In other words $\dot{M}$ the mass accretion rate, is the local value at $R_{\rm m}$. But mass can accumulate at the boundary layer (due to the centrifugal barrier), and the local mass accretion rate can be larger than the mass supply rate. This situation induces

an episodic accretion which had been explored by Spruit & Taam [12] and D'Angelo & Spruit [13, 14, 15].

The torque applied by the disk is;

$$N_{disk} = n(\omega_*)\dot{M}R_{\rm m}^2\Omega_K(R_{\rm m}). \tag{1.8}$$

where $n(\omega_*)$ defines dimensionless torque. Depending on the assumption of models there are numerous suggestions for $n(\omega_*)$ in the literature. The torque applied to the star is given as;

$$N_* = -2\pi I_* \frac{\dot{P}}{P^2}. \tag{1.9}$$

where I_* is the moment of inertia of the star and $\dot{P}$ is the spin period derivative of the star. Using 1.8 and 1.9, we get;

$$-\dot{P} = \frac{P^2}{2\pi}\frac{\dot{M}\left(GM_*R_{\rm m}\right)^{1/2}}{I_*}n(\omega_*). \tag{1.10}$$

If the inner radius of the disk is beyond the light cylinder, the disk can not apply a torque onto the star. When the inner radius goes beyond the light cylinder, the equilibrium between the magnetic pressure and the material pressure can not give a steady radius.

1.3.1 The Role of the magnetic field

In the absence of a disk the magnetic field lines are poloidal, $B_{\rm z} = \frac{\mu}{R^3}$, and azimuthal component of the field dominates at the equator plane. When a disk is introduced, the magnetic fields thread the disk and the magnetic field frozen into the plasma is then forced to follow the fluid elements in the ϕ-direction. Thus a toroidal field, B_ϕ, is generated. At the inner edge of the disk, some instabilities may occur (e.g. Kelvin-Helmholtz instability, Rayleigh-Taylor instability, reconnection, etc.) which may allow the penetration of the magnetic field to the disk. Stellar field lines penetrate the magnetospheric boundary by the help of the instabilities and gets twisted to produce the toroidal field $B_{\phi\pm} = \mp\gamma B_z$ where $\gamma \sim 1$ and upper and lower sign specifies the field above/below the disk. If the toroidal magnetic field becomes comparable to the poloidal field, the field lines will start to expand until they open up and the star disk linkage is broken and the opened field lines can cause outflows or reconnections [16, 17]. These suggestions were confirmed by [18, 19, 20, 21].

The position of the inner region of the accretion disk can be studied by observing quasi periodic oscillation (QPO). QPO, have been detected in the X-ray flux of the X-ray sources ranging from neutron stars to black hole candidates in LMXB. The QPO are generally assumed to result from the motion of inhomogeneous matter distribution in the inner region of the accretion disks and gives information about interaction between disk and compact star. A number of models are suggested to explain this phenomenon (see [22, 23, 24, 25, 26]).

1.4 Literature Summary

Over the last several decades numerous theoretical studies have been developed to understand the interaction between accretion disks and magnetized stars. According to the Ghosh & Lamb Model (1979) [8], stellar field lines penetrate the disk over a large range of radius. Differential rotation between the disk and the star will cause the field lines to wind up. In this theory, which is called magnetically threaded disk model (MTD), there is a steady state where the twisted field lines are balanced with dissipation, and at that point the field lines slip across the disk. The most important inadequacy of the model is that the arbitrarily large magnetic fields could build up by winding and such large toroidal fields could disrupt the disk [27]. It is possible that the stellar field lines can penetrate the disk only near the corotation radius, rather than a large range of radius [28]. Aly (1980) discussed the location of the magnetopause and the effect of non- radial magnetic force by assuming a perfectly conducting disk around the neutron star [29]. Anzer & Boerner (1980) showed that the differential rotation leads to Kelvin-Helmholtz instability and turbulent diffusion. So some part of the disk material falls on to the neutron star and the rest is flung out the system via these instabilities [30]. Wang (1987) found that the particular pitch distribution assumed by Ghosh & Lamb (1979) is not consistent since the resulting magnetic pressure would shatter the disk beyond the corotation radius [27]. Aly & Kuijpers (1990) put forward the idea that magnetic links are efficient transmitters of angular momentum. As the disk matter is close to the star, the field lines undergo a series of expansion and reconnection. They showed that these magnetic flares occur with a frequency a few times the beat frequency and are possible explanation for quasi periodic oscillation QPO [31]. Koenigl (1991) examined the dynamical and radiative consequences of disk

accretion onto magnetic T-Tauri stars by the help of Ghosh & Lamb model [32]. Spruit & Taam (1993) found that if the magnetospheric boundary is defined as the distance where rotation deviates from Kepler rate, there is a region inside boundary where the matter drifts inward by an interchange instability. So mass could be accreted in cyclic fashion by this instability [12]. Shu et al. (1994) examined the magneto-centrifugally driven flows from young stars and disks (X-wind model) [33]. Li et al. (1996) explored the formation of a standing accretion shock in steady-channeled accretion flows [34]. Lai (1998) constructed the magnetic slim disk models, involving the effects of both magnetic fields and general relativity [35]. Terquem & Papaloizou (2000) computed the warping of a disc resulting from an inclined dipole [36]. Shirakawa & Lai (2002) examined a global analysis of warping/precession modes in viscous accretion disks and showed that the magnetic warping torque can overcome viscous damping [37]. Pfeiffer & Lai (2004) carried out numerical simulations of the non-linear evolution of warped, viscous accretion disks driven by magnetic torques [38].

2. EXAMINATION OF THE DISK-MAGNETOSPHERE INTERACTION IN 4U 1626–67

2.1 Introduction

In order to understand long term evolution of the compact stars, it is important to know the relation between the torque acting on star and the fastness parameter.

Since neutron stars in LMXB have weak magnetic fields, the resulting disk torque on these objects is rather small. This makes it hard to observe the spin evolution in these systems. The spin evolution is easily observed in HMXB which include young neutron stars with strong magnetic fields, but accretion in these systems proceed by stellar winds rather than disks.

In order to study the disk torques we need to analyse a system with a small mass donor star and strongly magnetized neutron star. *4U 1626–67*, which accretes from low-mass donor star and hosts a neutron star with magnetic field, $\sim 10^{12}G$, is a good candidate to determine the relation between the torque and fastness parameter.

4U 1626–67 underwent two torque reversal in June 1990 and February 2008. We used the period, the period derivative and the flux evolution of *4U 1626–67* to find the dependence of the disk torque on the fastness parameter.

2.2 Method

The X-ray flux is defined as;

$$F_{\rm X} = \frac{L_{\rm X}}{4\pi b d^2} \tag{2.1}$$

where b is the beaming factor and the d is the distance of the star. Using 1.6, the mass flux accreting on the star is given as

$$\dot{M} = \frac{4\pi b d^2 F_{\rm X} R_*}{G M_*}. \tag{2.2}$$

Using the above equations in $R_{\rm m} = \xi R_{\rm A}$ where $R_{\rm A}$ is given in Eq.1.2, the magnetospheric radius or inner radius of the accretion disk;

$$R_{\rm m} = \xi \left(\frac{B^2 R_*^5 \sqrt{GM_*}}{16\sqrt{2}\pi b d^2 F_{\rm X}} \right)^{2/7} \tag{2.3}$$

where B is the magnetic field and we used $\mu = \frac{1}{2} B R_*^3$. Using Eq.2.3 and Eq.1.3 in Eq.1.5 the fastness parameter written as

$$\omega_* = \xi^{3/2} \left(\frac{B^2 R_*^5}{16\sqrt{2}\pi b d^2} \right)^{3/7} \frac{2\pi}{(GM_*)^{2/7} F_{\rm X}^{3/7} P}. \tag{2.4}$$

Accordingly, the critical fastness parameter at which the torque reversal occurs is

$$\omega_{\rm c} = \xi^{3/2} \left(\frac{B^2 R_*^5}{16\pi\sqrt{2} b d^2} \right)^{3/7} \frac{2\pi}{(GM_*)^{2/7} F_{\rm c}^{3/7} P_{\rm c}} \tag{2.5}$$

where $F_{\rm c}$ and $P_{\rm c}$ define the critical period and the critical flux, respectively. Using Eq.2.4 and Eq.2.5, we get;

$$x \equiv \frac{\omega_*}{\omega_{\rm c}} = \left(\frac{F_{\rm c}}{F_{\rm X}} \right)^{3/7} \left(\frac{P_{\rm c}}{P} \right). \tag{2.6}$$

Eq.1.9, together with Eq.1.6 and Eq.2.3 becomes

$$-\dot{P} = n \omega_*^{1/3} \frac{4\pi b d^2 R}{(2\pi)^{4/3} (GM_*)^{1/3} I} F_{\rm X} P^{7/3} \tag{2.7}$$

or using Eq.2.6 becomes

$$-\dot{P} = \frac{\omega_{\rm c}^{1/3} 4 b d^2 R_* F_{\rm c} P_{\rm c}^{7/3}}{(2\pi)^{4/3} (GM_*)^{1/3} I_*} \frac{n}{x^2}. \tag{2.8}$$

While the system near torque equilibrium, the dimensionless torque is written as $n = n_0(1-x)$. Using this approximation Eq.2.8 can be written in a different form;

$$-\dot{P} = C \frac{1-x}{x^2}, \qquad \text{for } x \simeq 1. \tag{2.9}$$

where

$$C \equiv \frac{\omega_c^{1/3} 4\pi b d^2 R F_{\rm c} P_{\rm c}^{7/3} n_0}{(2\pi)^{4/3} (GM_*)^{1/3} I_*} \tag{2.10}$$

is a constant. Using the slope of $\dot{P}$ versus $(1-x)/x^2$, C is found and the value of C is substituted in Eq.2.8 and one finds;

$$\frac{n}{n_0} = -\frac{\dot{P} x^2}{C}. \tag{2.11}$$

2.3 Application to 4U 1626–67

4U 1626–67 is discovered by UHURU [39] it is a LMXB including a 7.66 s X-ray pulsar [40]. The pulse frequency history is given by 1 and in this Figure, the torque reversals in June 1990 and in February 2008 can be seen, clearly [41].

The period evolution is seen Figure 2.1. In order to obtain more data points, observational data represented by dots [41] are smoothed by interpolation.

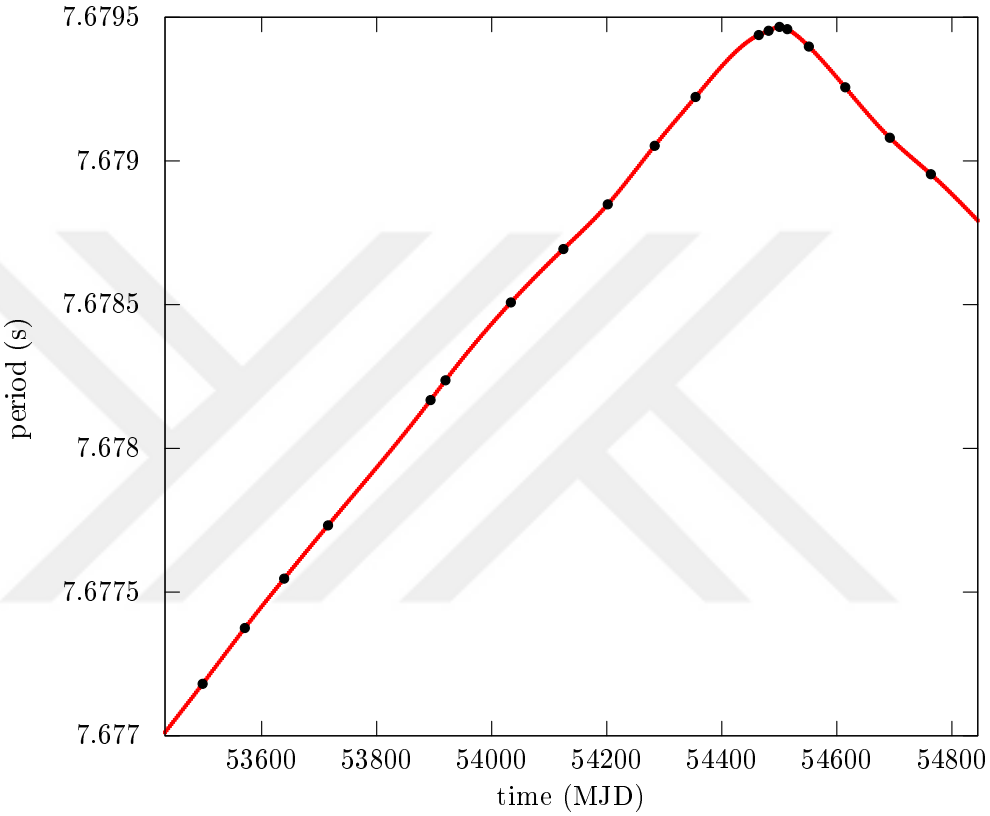

Figure 2.1 : Period evolution of *4U 1626–67*.

The flux evolution is seen Figure 2.2. Observational data represented by dots [41] are smoothed in a similar way.

In Figure 2.1, the critical period at which the torque reversal is observed is seen to be $P_c = 7.67946628$ s. In Figure 2.2, the critical flux at which the torque reversal is observed is seen to be $F_c = 0.00658$ c*nt* cm^{-2} s^{-1}.

Using Eq.2.6, the observational data can be converted a series form of x.

In Figure 2.3, one can see the $\dot{P}$ data and using these data, the constant C in Eq.2.9 can be found.

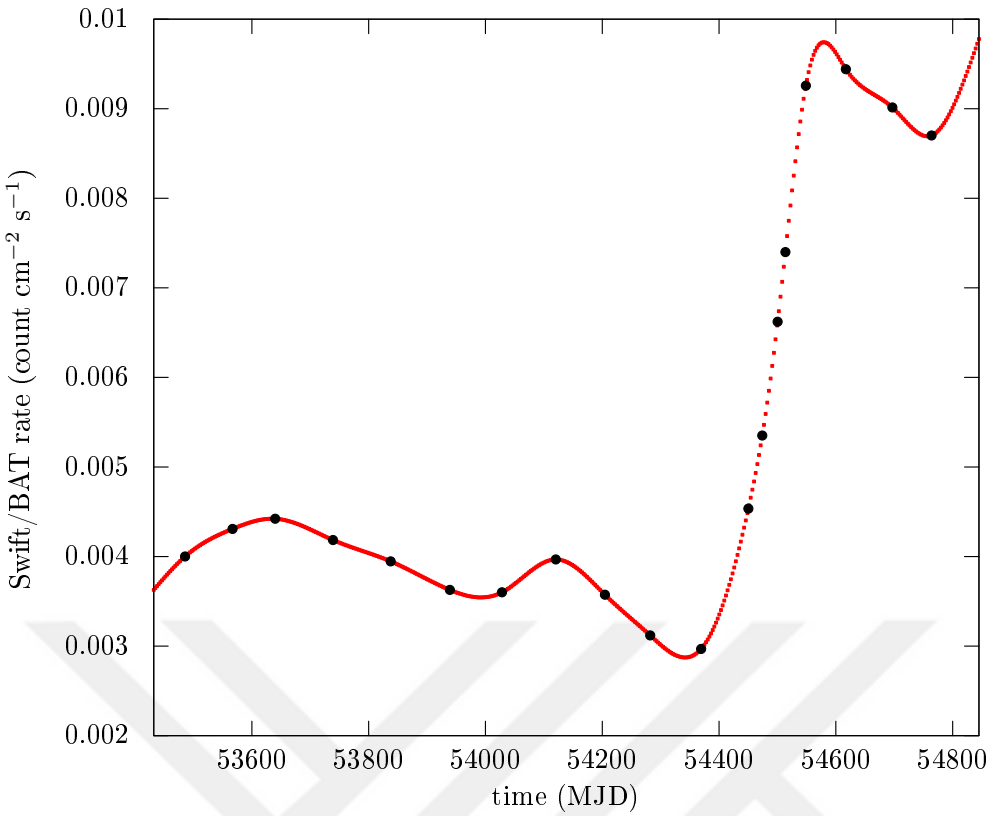

Figure 2.2 : Flux evolution of *4U 1626–67*.

In Figure 2.4, the plot of $\dot{P}$ versus $(1-x)/x^2$ is seen. Using the slope of this graphic C is found as, $C \simeq 9 \times 10^{-11}$.

2.4 Results and Discussions

In Figure 2.5, the relation between the dimensionless torque scaled with n_0 and fastness parameter, ω_*, is shown .

As seen, while the torque models in the literature [42] have a convex shape near torque equilibrium, the torque that we obtained using observational data of *4U 1626–67* can be defined as a cubic function, in the range of $x = 0.8 - 1.1$;

$$\frac{n}{n_0} = 1 - x - a(x-1)^2 - b(x-1)^3 \tag{2.12}$$

where a $= 11.0946 \pm 0.1787(1.61\%)$ and b $= 55.7817 \pm 0.9935(1.78\%)$.

The torque models shown in Figure 2.5 .

According to Ghosh & Lamb Model [8], the dimensionless torque is defined as;

$$n_{GL} = 1.39 \frac{1 - \{\omega_*[4.03(1-\omega_*)^{0.173} - 0.878]\}}{1-\omega_*} \tag{2.13}$$

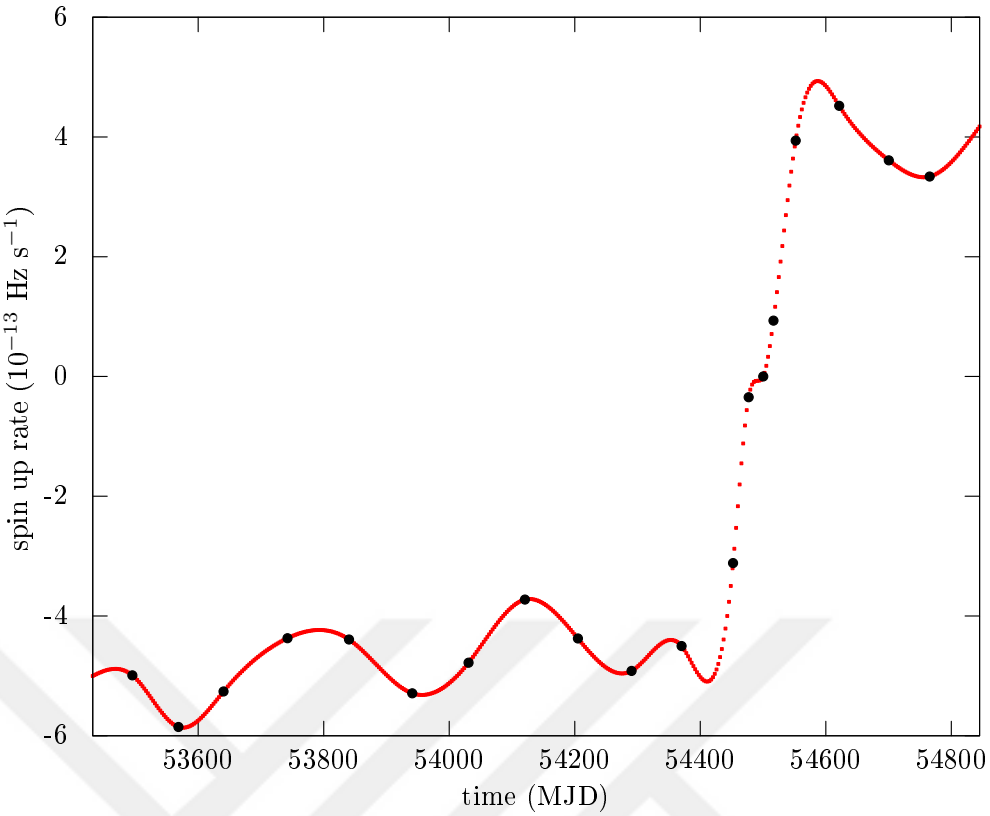

Figure 2.3 : Period derivative evolution of *4U 1626–67*.

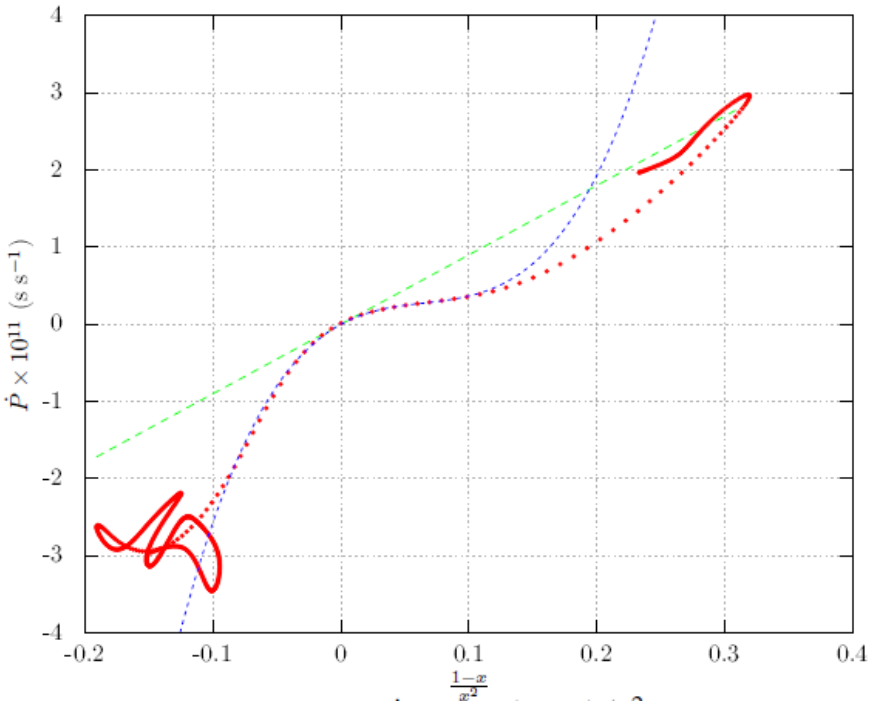

Figure 2.4 : $\dot{P}$ versus $(1-x)/x^2$.

for which $\omega_c = 0.35$ [8]. In order to compare our model with Ghosh & Lamb Model, we used x $= \omega_*/\omega_c$. So;

$$\frac{n_{GL}}{n_0} = 0.737 \frac{1 - \{\omega_c x[4.03(1-\omega_c x)^{0.173} - 0.878]\}}{1-\omega_c x}. \tag{2.14}$$

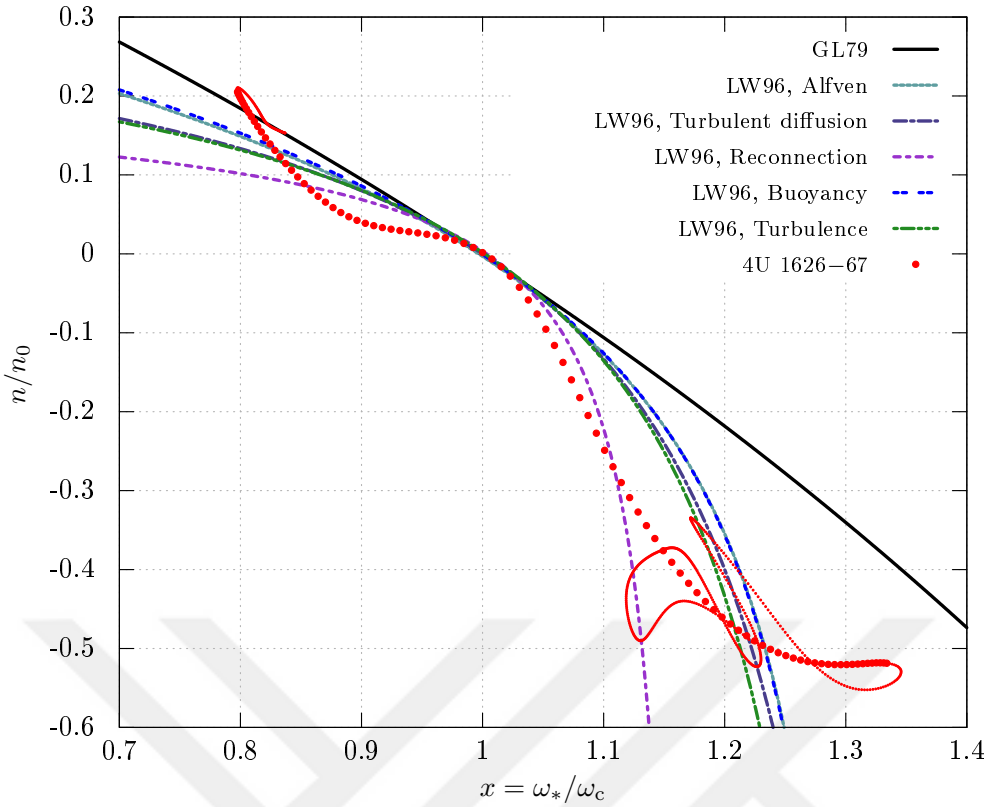

Figure 2.5 : The dimensionless torque scaled with n_0 versus ω_*.

Table 2.1 : The torque models given by [42].

$n(x) =$	physics limiting B_ϕ	ω_c	n_0
$1+\frac{8}{9}\left(1-\omega_c x-\frac{(\omega_c x)^{57/40}}{(1-\omega_c x)^{1/2}}\right)$	Alfvén speed	0.76	4.3673
$\frac{(5/3)-(7/3)\omega_c x}{1-\omega_c x}$	turbulent diffusion	5/7	35/6
$\frac{(5/3)-(7/3)\omega_c x+(4/9)\omega_c^2 x^2}{(1-\omega_c x)}$	reconnection	0.85	8.7728
$1+\frac{8}{9}\left(1-\omega_c x-\frac{(\omega_c x)^{35/24}}{(1-\omega_c x)^{1/2}}\right)$	buoyancy	0.76	4.3242
$1+\frac{20}{31}\frac{1-(31/16)\omega_c x}{1-\omega_c x}$	turbulence	0.73	6.0567

The torque models are obtained by different assumptions. Different disk-magnetosphere interactions can restrict the growth of the toroidal field generated by differential rotation between the magnetosphere and the disk, for example, turbulent diffusion, Alfvén speed, reconnection, buoyancy and turbulence [42]
where $n_0 = -n'_{GL}(1) = 1.8839$.

In Figure 2.5, the solid black curve defines Ghosh & Lamb Model [8].

2.5 Conclusions

It is seen that the torque model inferred from the observational data of *4U 1626–67* is quite different than the existing torque models in the literature. The models in the literature have convex shape in the vicinity of torque equilibrium. But in the observational result, the torque acting on the star can be fitted with at least a cubic function and behaves as a concave-up shape. Beyond the equilibrium, the torque-fastness relation is irregular. This possibly indicates, an unstable regime that is triggered when the inner radius is close to the corotation radius. But the physics of the erratic behavior of the fastness parameter at slow-rotating limit is unclear. Thus, inadequacies of MTD model are displayed.

3. NEUTRON STAR MODEL FOR PULSATING ULTRALUMINOUS X-RAY SOURCES

3.1 Introduction

Some of the galaxies close to our galaxy host several ultraluminous X-ray sources ULX that contain compact objects whose luminosities far exceeds the Eddington limit and whose mass exceed a solar mass. The initial assumption that the observed luminosity is isotropic led to the view that such systems host intermediate-mass black holes of mass $\sim 100M_{\odot} - 10^4 M_{\odot}$ (see e.g. [43, 44, 45, 46]). Many other studies have hypothesized that ULX is home to stellar-mass black holes with anisotropic radiation that slightly exceeds the Eddington limit [47, 48, 49].

Discovery of pulsating ultraluminous X-ray sources PULX, (*M82* [50], *NGC 5907* [51], *NGC 7793* [51], *NGC 300* [52], *NGC 1313* [53], *M51* [54]) point out that PULX harbor neutron stars rather than black holes, and are more common in the ULX population ([55, 56, 57, 58, 59]). Bachetti et al.(2014) explained the super Eddington luminosity of the first PULX that they discovered with the fan-beam geometry displayed at an appropriate angle ([60]) and based on their method, they calculated the magnetic field of the neutron star as $B = 10^{12}$ G.

Ekşi et al. [61] using the spin-up rate of the object inferred that, the neutron star in this system has super strong magnetic fields ($B \gtrsim B_c = 4.4 \times 10^{13}$ G) that reduce the scattering cross section and increase the critical luminosity ([62], [63], [64]). Dall'Osso et al. (2015), [65], and Tsygankov et al. (2016), [66], obtained magnetic field values compatible with the results obtained by Ekşi et al. (2015). Israel et al. (2017a), [51], suggested that, as Ekşi et al. (2015) suggested, the observed properties of PULX in *NGC 5907* can only be explained by the presence of super-strong quadrupole fields. King and Lasota (2019), [67], argued that systems with strong magnetic fields such as magnetars are unlikely to occur in binary systems, and ULX systems are no exception. Based on the beaming of outflow and spherization of the

disk in supercritical accretion, King and Lasota (2019) found the magnetic fields in the range of $\sim 10^{11} - 10^{13}$ G. Kluzniak and Lasota (2015), [68], and Christodoulou et al. (2018), [69], assumed that such systems have even much weaker magnetic fields, $B \sim 10^{10}$ G, assuming that the discovered PULX is not in spin equilibrium. If the magnetic field strength is of this order, the magnetosphere surrounded by Eddington mass flux or a higher mass flux will not allow any pulse to be observed. Brightman et al. (2018), [70], calculated the magnetic field strength of 10^{15} G when the 4.5 keV line discovered in the spectrum of ULX in *M51* is due to proton scattering, or corresponds to a 10^{11} G magnetic field where it is caused by electron scattering. However, assuming that the cyclotron line originates from the accretion column rather than the stellar surface, stronger field estimates can be obtained. Based on the *PULX NGC 300 ULX1* source having a potential cyclotron property at about 13 keV, Walton et al. (2018), [71] suggested that this source has a magnetic field of $B \sim 10^{12}$ G. These observations are consistent with the surface areas of $B \sim 10^{13}$ G obtained in the strong spin-up state, assuming electron cyclotron resonance spectral properties occurring in an accretion column a few times the radius of the star.

According to the evolutionary model developed by Erkut et al. (2019), [72], for ULX, some newborn neutron stars with magnetic field intensities in the range of $10^{11} - 10^{15}$ G can interact with wind-fed discs in HMXB and so are seen as pulsating and non-pulsating ultraluminous sources. If the system is in the propeller stage, the rapidly rotating neutron star magnetosphere prevents material transfer onto the system, and the system turns into a nonpulsating ULX. Systems with initial magnetic fields $\sim 10^{11}$ G take 10^5 years to go through the supercritical propeller phase, appearing as ULX with the typical luminosity of ultra-light super soft sources. However, systems with magnetic fields in the range of $10^{13} - 10^{15}$ G are likely to appear as PULX during the long accumulation stage that they must pass during their lifetimes [72].

In this thesis, we treat PULX as neutron stars that accumulate mass at super Eddington ratios from their companions in HMXB. We also calculate the surface magnetic field of the neutron star by examining the torque and luminosity states of the PULX. We also estimate ranges for beaming fraction and fastness parameters. From the results, we

predict that many ULX host neutron stars whose beamed X-ray luminosities coincides with with our line of sight, causing the super Eddington luminosity to appear.

3.2 Method

3.2.1 Inner radius

We assume that the X-ray luminosity arises from the gravitational energy released by accretion onto the neutron star: $L_{\rm X} = GM_*\dot{M}_*/R_*$, where $\dot{M}_*$ is the mass accretion rate onto the neutron star of mass M_* and radius R_* [7]. Assuming that the X-ray emission is beamed by a factor $b < 1$, the X-ray flux at a source distance d is then $F_{\rm X} = L_{\rm X}/4\pi bd^2$, Equation 2.1. Accordingly, the mass accretion rate onto the neutron star can be estimated as

$$\dot{M}_* = \frac{4\pi bR_* d^2 F_{\rm X}}{GM_*}. \tag{3.1}$$

We assume the mass donor is at a stage such that it transfers matter at a super-Eddington rate, $\dot{M}_0 > \dot{M}_{\rm E} \equiv L_{\rm E}/\varepsilon c^2$, where $\varepsilon \simeq 0.1$ is the efficiency of gravitational energy release and $L_{\rm E}$ is the Eddington luminosity defined in Equation 1.7.

The supercritical mass flow within the disk makes the accretion flow quasi-spherical in a region known as the spherical radius and within the spherization radius, the disk is geometrically and optically thick.

$$R_{\rm sp} = \frac{27\varepsilon\sigma_{\rm T}\dot{M}_0}{8\pi m_{\rm p}c} \simeq 1.43\times10^9\ {\rm cm}\ \varepsilon\left(\frac{\dot{M}_0}{10^{20}\,{\rm g\,s^{-1}}}\right) \tag{3.2}$$

determined by $L(R > R_{\rm sp}) = 27\varepsilon GM_*\dot{M}_0/2R_{\rm sp} = L_{\rm E}$ and the flow regulates itself so that the local Eddington rate is not exceeded, i.e.,

$$\dot{M} = \begin{cases} \dot{M}_0(R/R_{\rm sp}), & \text{for } R < R_{\rm sp}; \\ \dot{M}_0, & \text{for } R > R_{\rm sp}. \end{cases} \tag{3.3}$$

[5].

Since viscous stresses are negligible in the inner radius of the disk, the inner radius of the disk is determined by the balance between magnetic and material stresses [8],

$$\frac{d}{dR}\left(\dot{M}R^2\Omega\right) = -R^2B_\phi^+B_z, \tag{3.4}$$

where Ω is the angular velocity of the innermost disk matter within the boundary region, B_z is the poloidal magnetic field, $B_\phi^+ = \gamma_\phi B_z$ is the toroidal magnetic field at the surface of the disk and γ_ϕ is the azimuthal pitch of order unity.

Integrating Equation 3.4 with the aid of Equation 3.3 over the narrow zone (boundary region), where the neutron-star magnetosphere threads the inner disk, we write

$$\frac{\dot{M}_0 R_{\rm in}^3 \left[\Omega_{\rm K}\left(R_{\rm in}\right) - \Omega_*\right]}{R_{\rm sp}} = -\int_{R_{\rm in}-\Delta R}^{R_{\rm in}} \gamma_\phi B_z^2 R^2 dR, \tag{3.5}$$

taking into account that $\Omega\left(R_{\rm in}\right)$ and $\Omega\left(R_{\rm in} - \Delta R\right)$ can be approximated by the Keplerian angular velocity at the inner radius, $\Omega_{\rm K}\left(R_{\rm in}\right)$, and the angular velocity of the neutron star, Ω_*, respectively. The right hand side of this equation is of the form $\mu^2\delta/R_{\rm in}^3$, where μ is the magnetic dipole moment of the neutron star and $\delta = \Delta R/R_{\rm in}$ is the relative width of the coupled domain (boundary region) between the disk and the neutron-star magnetosphere.

The azimuthal pitch can be expressed in terms of the rotational shear between the magnetosphere and the innermost disk matter as $\gamma_\phi \simeq \omega_* - 1$, where ω_* is the fastness parameter defined in Equation 1.5, [73]. Assuming that $B_z \simeq -\mu/R_*^3$, it then follows from Equation 3.5 that

$$R_{\rm in} = \left(\frac{\mu^2 R_{\rm sp}\delta}{\dot{M}_0\sqrt{GM_*}}\right)^{2/9}, \tag{3.6}$$

which defines the inner radius of a disk around a magnetized neutron star accreting at super-critical rates. In the steady state, the mass flux at the inner disk equals the mass flux onto the star. Substituting $\dot{M}_* = \dot{M}_0\left(R_{\rm in}/R_{\rm sp}\right)$ into Equation 3.1, we can rewrite the inner disk radius in Equation 3.6 as

$$R_{\rm in} = \left(\frac{\mu^2\sqrt{GM_*}\delta}{4\pi b R_* d^2 F_{\rm X}}\right)^{2/7}. \tag{3.7}$$

This expression is not explicit as it depends on b, which in turn might depend on the inner radius of the disk. In the next subsection, we determine b in terms of $R_{\rm in}$ to obtain a self-consistent solution.

3.2.2 Beaming fraction

We assume here that the beaming fraction, b, is determined by the opening angle of the polar cap and therefore the fractional area of the polar region as

$$b = \frac{A_{\rm c}}{\gamma A}, \tag{3.8}$$

where $A_{\rm c}$ is the polar cap area, $A = 4\pi R_*^2$ is the total surface area of the neutron star, and $\gamma < 1$ is a normalization constant corresponding to the maximum fractional area of the polar cap.

The definition of beaming fraction proposed by King [47] depends only on the mass transfer ratio. However, beaming fraction, if pulsating source are to be addressed, is not only dependent on the mass transfer rate, but also on the magnetic field and the angle of inclination of the source. In addition, since it is known that the pulsation stem from most sources is caused by the disc-magnetosphere interaction, the definition of beaming we put forward is a more reliable definition.

The size of the polar cap can be inferred as follows: Dipole field lines in polar coordinates are defined as $r = C\sin^2\theta$. Assuming that the inclination angle between the rotation and magnetic axes is α, the field line that connects the inner edge of the disk to the star is described by $r = R_{\rm in}\sin^2\theta/\cos^2\alpha$. This field line makes an angle $\theta_{\rm c}$ with the magnetic axis on the neutron-star surface such that $\sin\theta_{\rm c} = \sqrt{R_*/R_{\rm in}}\cos\alpha$. The ratio of the polar cap area to the surface area of the neutron star is $A_{\rm c}/A = \frac{1}{2}(1-\cos\theta_{\rm c})$. For $R_* \ll R_{\rm in}$ ($\sin\theta_{\rm c} \simeq \theta_{\rm c}$ and $\cos\theta_{\rm c} \simeq 1-\theta_{\rm c}^2/2$), as would be valid for a strongly magnetized neutron star, we simplify the same ratio as

$$\frac{A_{\rm c}}{A} \simeq \frac{R_*}{4R_{\rm in}}\cos^2\alpha \tag{3.9}$$

[9].

Substituting the above result into Equation 3.8, we obtain $b = \left(\cos^2\alpha/4\gamma\right)R_*/R_{\rm in}$. Expressing $\mu = BR_*^3/2$ in terms of the polar surface field strength B, it follows from Equation 3.7 that

$$R_{\rm in} = \left(\frac{\gamma\sqrt{GM_*}B^2R_*^4\delta}{4\pi d^2\cos^2\alpha\, F_{\rm X}}\right)^{2/5} \tag{3.10}$$

for the inner disk radius and

$$b = \left(\frac{\pi d^2 \cos^7 \alpha \, F_{\rm X}}{8\gamma^{7/2} \sqrt{GM_*} B^2 R_*^{3/2} \delta} \right)^{2/5} \tag{3.11}$$

for the beaming fraction, which can be used in Equation 3.1 to find

$$\dot{M}_* = \left[\frac{4\pi^{7/2} d^7 \cos^7 \alpha \, R_* F_{\rm X}^{7/2}}{\gamma^{7/2} \left(GM_*\right)^3 B^2 \delta} \right]^{2/5} . \tag{3.12}$$

Note from Equation 3.12 that the mass accretion rate, $\dot{M}_*$, and the X-ray flux, $F_{\rm X}$, are not linearly proportional as a consequence of beaming. An increase in $\dot{M}_*$ does not imply an increase in $F_{\rm X}$ at the same ratio. This is because a higher $\dot{M}_*$ results in a smaller inner radius, which increases the polar cap area and hence the beaming fraction.

The fastness parameter defined by Equation 1.5 can also be expressed in an explicit form with the use of Equation 3.10 for the inner disk radius and $R_{\rm co} = (GM_* P^2/4\pi^2)^{1/3}$ for the corotation radius. We find

$$\omega_* = \left(\frac{\gamma \sqrt{GM_*} B^2 R_*^4 \delta}{4\pi d^2 \cos^2 \alpha F_{\rm X}} \right)^{3/5} \frac{2\pi}{P\sqrt{GM_*}} \tag{3.13}$$

for the fastness parameter.

Using Equation 3.1 and Equation 3.11, we write the beaming fraction in terms of the mass accretion rate onto the neutron star and the model parameters such as α and γ as

$$b \simeq 0.0011 \, \frac{\cos^2 \alpha}{\gamma} \left(\frac{M_{1.4} \dot{M}_{18}^2}{R_{10}^5 B_{13}^4 \delta_{0.1}^2} \right)^{1/7} , \tag{3.14}$$

where $M_{1.4} \equiv M_*/1.4 M_\odot$, $R_{10} \equiv R_*/10\,{\rm km}$, $\dot{M}_{18} \equiv \dot{M}_*/10^{18}\,{\rm g\,s^{-1}}$, $B_{13} \equiv B/10^{13}\,{\rm G}$, and $\delta_{0.1} \equiv \delta/0.1$. In Figure 3.1, we display the variation of the beaming fraction with γ (normalization constant) for the wide ranges of $\dot{M}_*$ and B. Given a certain value of γ, the systems with low $\dot{M}_*$ and high B have lower beaming fractions compared to those with high $\dot{M}_*$ and low B.

There is yet to be a direct observational clue about the inclination angle, α , and the normalization constant γ. Therefore, the estimation of the magnetic field based on the α and the γ can be tricky. We will express the magnetic field and fastness parameter depending on the beaming fraction, without reference to the α and the γ (see

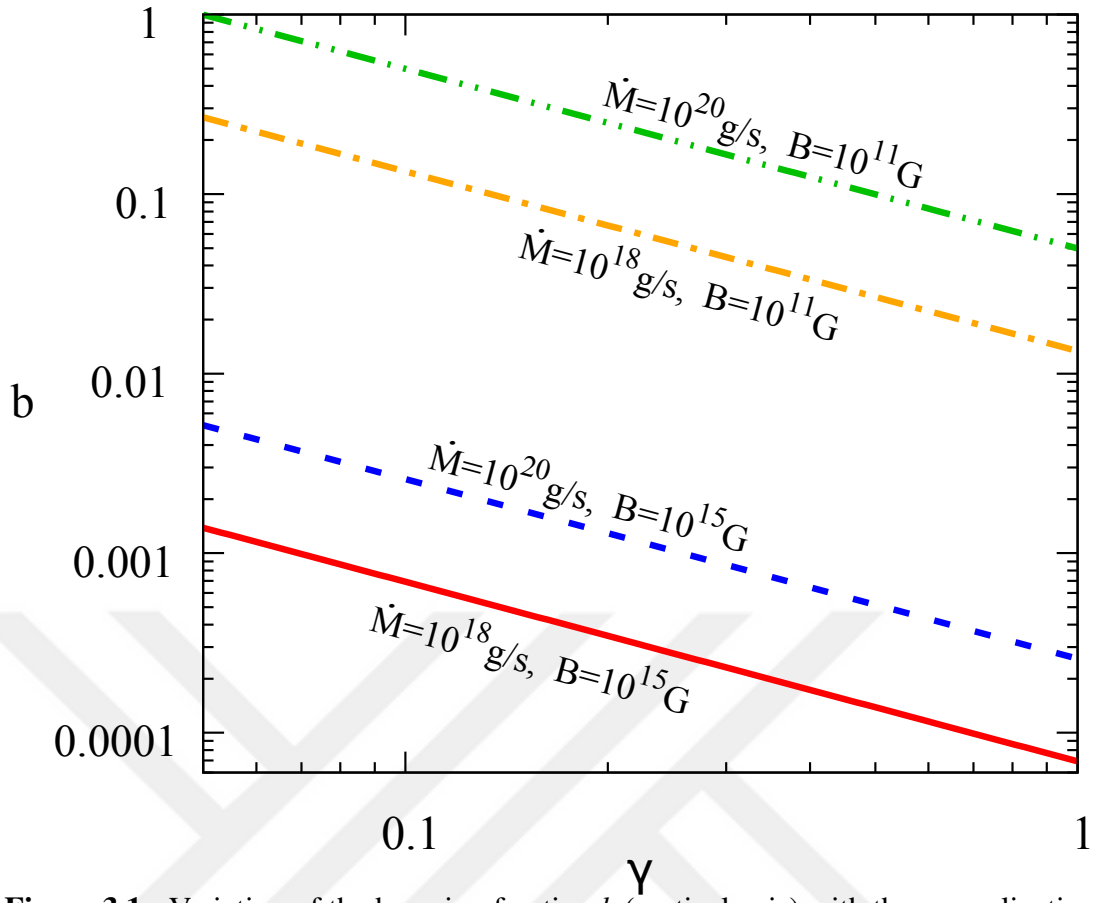

Figure 3.1 : Variation of the beaming fraction b (vertical axis) with the normalization constant γ (horizontal axis) for the 10^{18}–$10^{20}\,\mathrm{g\,s^{-1}}$ range of $\dot{M}_*$ and 10^{11}–$10^{15}\,\mathrm{G}$ range of B. Here, the boundary region width is selected as $\delta = 0.1$. In addition, the mass, the radius and the inclination angle between rotation and magnetix axis of the neutron star are selected as $M_* = 1.4M_\odot$, $R_* = 10$ km and $\alpha = 20^\circ$ respectively [74].

Equation 3.15 and Section 3.3). Using Equation 3.11 and Equation 3.13, we eliminate γ to obtain

$$B = \frac{2^{5/6}\,(GM_*)^{1/3}\,(P\omega_*)^{7/6}\,d\sqrt{F_X b}}{\pi^{2/3}R_*^{5/2}\sqrt{\delta}} \tag{3.15}$$

for the dipolar magnetic field strength on the surface of the neutron star. Note that the expression for B in Equation 3.15 does not depend on how we model the beaming fraction (Equation 3.15 does not contain the specific parameters such as α and γ we use to define b and could also be obtained using Equation 1.5 and Equation 3.7 and will therefore be used further in our analysis.

3.3 Inference of Magnetic Field From Torque and Luminosity

In this section, we estimate the magnetic field strengths of PULX using different methods based on the accretion torque acting on the neutron star and the maximum critical value of the X-ray luminosity. Throughout our analysis, we employ $M_* = 1.4M_\odot$, $R_* = 10$ km, and $I = 10^{45}\,\mathrm{g\,cm^2}$ for the neutron-star mass, radius, and moment of inertia, respectively.

Table 3.1 : Observed periods, period derivatives (spin-up), X-ray fluxes, and distances of PULX.

Source	$P\,(\mathrm{s})$	$\dot{P}\left(\mathrm{s\ s^{-1}}\right)$	$F_\mathrm{X}\left(\mathrm{erg\ s^{-1}cm^{-2}}\right)$	$d\,(\mathrm{Mpc})$	References
NGC 5907	1.137	-5×10^{-9}	4.29×10^{-12}	17.1	[51]
NGC 7793 P13	0.417	-2×10^{-12}	5.19×10^{-12}	3.9	[75]
M82 X-2	1.37	-2×10^{-10}	4.18×10^{-12}	3.6	[50]
NGC 300 ULX1	31.6	-5.56×10^{-7}	1.11×10^{-11}	1.88	[52]
M51 ULX-7	2.798	-2.4×10^{-10}	7.95×10^{-13}	8.58	[54]
NGC 1313 X-2	1.458	-1.38×10^{-8}	9.43×10^{-12}	4.2	[53]
Swift J0243.6+6124	9.833	-2.3×10^{-8}	2.90×10^{-7}	0.007	[76]

3.3.1 Magnetic field inferred from spin-up rate

We write the accretion torque acting on the neutron star as $N = n\dot{M}_*\sqrt{GM_*R_\mathrm{in}}$, where n is the dimensionless torque. Using the observed spin periods, P, and period derivatives, $\dot{P}$, we solve the torque equation $N = I\dot{\Omega}_*$ to estimate the magnetic field of the neutron star of moment of inertia I. If the system is away from spin equilibrium, the dimensionless torque can be approximated as $n = n_0$, where n_0 is a constant of order unity. Next, we employ Equation 1.5 to write the torque equation as

$$-2\pi I\dot{P}/P^2 = \omega_*^{1/3} n_0 \sqrt{GM_*R_\mathrm{co}}\dot{M}_*. \tag{3.16}$$

Solving Equation 3.13 for B, it follows from Equation 3.12 that

$$\dot{M}_* = \frac{\pi R_*^2 F_\mathrm{X} d^2 \cos^2\alpha}{\gamma (GM_*)^{4/3}} \left(\frac{2\pi}{\omega_* P}\right)^{2/3}, \tag{3.17}$$

which we exploit in Equation 3.16 to obtain

$$\gamma = \left(\frac{\pi}{4}\right)^{1/3} \frac{n_0 F_X P^{5/3} \left(R_* d \cos\alpha\right)^2}{I|\dot{P}| \left(GM_*\right)^{2/3} \omega_*^{1/3}}. \tag{3.18}$$

Substituting Equation 3.18 into Equation 3.13 and Equation 3.11, we estimate the magnetic field and the fastness parameter in terms of the beaming fraction and the measured quantities such as P, $\dot{P}$, F_X, and d in Table 3.2 as

$$B = \frac{\omega_*}{R_*^3} \sqrt{\frac{2GM_* I|\dot{P}|}{\pi n_0 \delta}} \tag{3.19}$$

and

$$\omega_* = \frac{\pi GM_*}{4} \left(\frac{I|\dot{P}|}{n_0 F_X d^2 P^{7/3} R_* b}\right)^3, \tag{3.20}$$

respectively. The expressions in Equation 3.19 and Equation 3.20 could also be obtained substituting Equation 3.1 and Equation 3.15 into Equation 3.16. Our results do not depend on the modelling of the beaming fraction in terms of the specific parameters such as α and γ we introduced in Equation 3.8 and Equation 3.9.

The shaded regions in each panel in Figure 3.2 show the allowed magnetic field values. Magnetic field values are determined by the maximum and minimum values of the boundary region thickness, δ. It has been assumed that the thickness of the boundary region varies between $\delta \simeq 0.01$ to $\delta \simeq 0.3$, [77]. The weak magnetic fields correspond to the smallest value of the fastness parameter, while the highest value of the fastness parameter, $\omega_* = 1$, gives the strong magnetic field values. Examining Equation 3.19 and Equation 3.20, it can be seen that the weak magnetic fields correspond to the upper limit of beaming fraction. However, the upper limit of the fastness parameter $(\omega_* = 1)$ corresponds to the lower limit of beaming fraction b and gives the strong magnetic field values. All possible situations and the results for the magnetic field ranges inferred from spin up rates are shown in Figure 3.2 and Table 3.2, respectively. There are two situations that we want to emphasize in Figure 3.2. As can be seen in Figure 3.2, we examined the M51 ULX-7 source for two different mass values. The fastness parameter and magnetic field value corresponding to $M_* = 1.4M_\odot$ value is at least one order of magnitude smaller than the values that we find for $M_* = 2M_\odot$. This situation shows us that as the mass of the neutron star gets smaller, the value of the fastness parameter can decrease. Secondly, taking $M_* = 1.4M_\odot$ and $R_* = 10$ km for NGC 1313 X-2 source, a solution corresponding to the situation for $\omega_* < 1$ could not

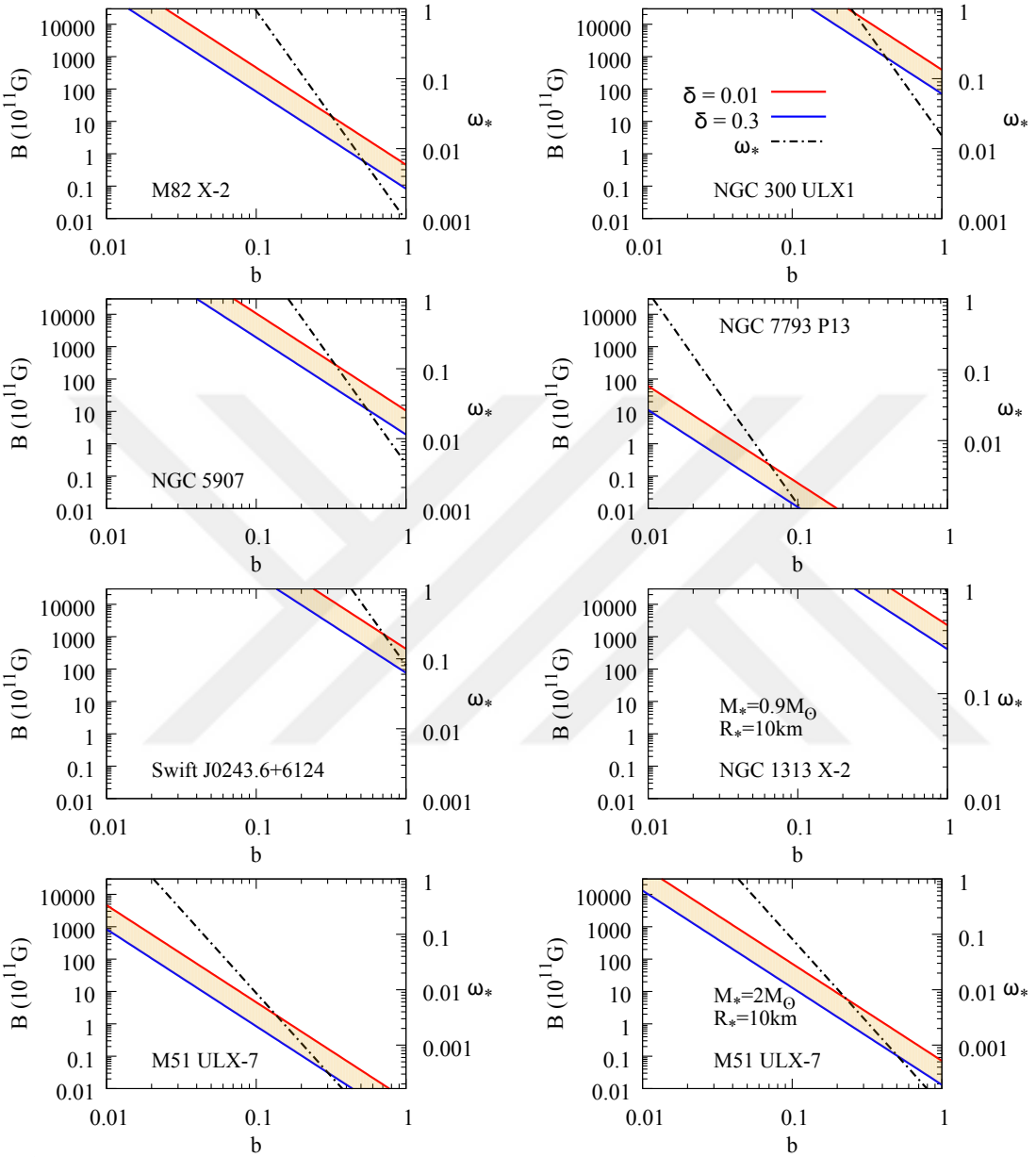

Figure 3.2 : Here, the magnetic field and fastness parameter values are expressed in terms of beaming fraction. The red and the blue solid curves correspond to values $\delta = 0.01$ and $\delta = 0.3$, respectively. The fastness parameter is shown with the dotted dashed curve. We use $M_* = 1.4M_\odot$ and $R_* = 10$ km for all sources. The bottom-left and-right panels for M51 ULX-7 compare two different cases with $M_* = 1.4M_\odot$ and $M_* = 2M_\odot$, respectively, [74].

be found. Therefore, by taking the values of $M_* = 0.9M_\odot$ and $R_* = 10$ km, marginal solutions corresponding to the values for $b \simeq 1$ and $\omega_* \simeq 1$ were obtained.

Table 3.2 : Weakest (min) and strongest (max) magnetic field ranges inferred from spin-up rates.

Source	$B_{min}(\times 10^{11}\mathrm{G})$	$B_{max}(\times 10^{13}\mathrm{G})$
ULX NGC 5907	$2.0-10$	$4.0-25$
ULX NGC 7793 P13	$0.012-0.070$	$0.09-0.5$
M82 X-2 (J095551+6940.8)	$0.08-0.5$	$0.80-5.0$
NGC 300 ULX1	$70-400$	$45-240$
M51 ULX-7	$0.018-0.090$	$1.0-6.0$
NGC 1313 X-2	$400-2300$	$4.6-25$
Swift J0243.6+6124	$80-240$	$10-50$

Here the magnetic field range of NGC 1313 X-2 are marginally obtained at $b \simeq 1$ for $M_* = 0.9M_\odot$ and $R_* = 10$ km. For all other sources we use $M_* = 1.4M_\odot$ and $R_* = 10$ km .

3.3.2 Magnetic field inferred from spin equilibrium

The short spin-up time scales $P/\dot{P} \sim 100$ yrs of PULX [50, 51, 75] means that the neutron stars in such systems must have reached spin equilibrium with their discs. This allows for an estimation of the magnetic field as was inferred for millisecond pulsars [78]. If the disk is in outburst state, which corresponds to an enhanced mass transfer rate at the time of observation, as in the PULX in M82, the spin equilibrium assumption is not valid [66]. It is assumed that the system approaches spin equilibrium at a critical fastness parameter, $\omega_c \lesssim 1$. In this case, all torque models near the spin equilibrium behave as $n \propto 1 - \omega_*/\omega_c$. In the case of spin equilibrium $\omega_* = \omega_c$, the inner radius of the disc approaches the corotation radius by $R_{in} = \omega_c^{2/3} R_{co}$. Assuming that the fastness parameter constant at the critical value, $\omega_c = 0.75$, [79], in the Equation 3.15, the magnetic field, B, can be expressed in terms of beaming fraction, b. When the Equation 3.15 is examined, it can be seen that strong magnetic fields correspond to the $(b = 1)$. In order to find the minimum value of beaming fraction b corresponding to weak magnetic fields, we considered the super Eddington mass transfer rate condition.

Using Equation 3.3, we write

$$\dot{M}_0 = \left(\frac{R_{\rm sp}}{\omega_{\rm c}^{2/3} R_{\rm co}} \right) \dot{M}_* > \frac{L_{\rm E}}{\varepsilon c^2}, \tag{3.21}$$

where $R_{\rm sp} = 27\varepsilon G M_* \dot{M}_0 / 2L_{\rm E}$. Substituting Equation 3.1 for $\dot{M}_* \equiv \dot{M}(R_{\rm in})$, it follows from Equation 3.21 that

$$b \gtrsim 0.3 \frac{P^{2/3}}{F_{11} d_1^2 \dot{M}_{20}} \tag{3.22}$$

provided $\varepsilon = 0.1$ and $\omega_{\rm c} = 0.75$. Here, P is the spin period in seconds, F_{11} is the X-ray flux in units of $10^{-11}\,{\rm erg\,s^{-1}\,cm^{-2}}$, d_1 is the distance in Mpc, and $\dot{M}_{20}$ is $\dot{M}_0$ in units of $10^{20}\,{\rm g\,s^{-1}}$. We expect from $R_{\rm co} \approx R_{\rm sp}$ that $P^{2/3}/\dot{M}_{20} \approx 0.85$ and therefore

$$b \gtrsim 0.25 F_{11}^{-1} d_1^{-2}. \tag{3.23}$$

Table 3.3 : Weakest (min) and strongest (max) magnetic field ranges inferred from spin equilibrium. For all sources we use $M_* = 1.4 M_\odot$ and $R_* = 10$ km .

Source	$B_{min}(\times 10^{13}{\rm G})$	$B_{max}(\times 10^{14}{\rm G})$
ULX NGC 5907	$0.24 - 1.4$	$0.80 - 4.5$
ULX NGC 7793 P13	$0.077 - 0.42$	$0.061 - 0.33$
M82 X-2 (J095551+6940.8)	$0.30 - 1.7$	$0.20 - 1.0$
NGC 300 ULX1	$12 - 67$	$7.0 - 35$
M51 ULX-7	$0.70 - 3.9$	$0.50 - 2.6$
NGC 1313 X-2	$0.35 - 1.8$	$0.40 - 2.1$
Swift J0243.6+6124	$3.2 - 17$	$1.0 - 5.7$

Using the observed values of $F_{\rm X}$ and d in Table 3.2, we obtained the minimum value of b for each PULX (see Equation 3.23). In Table 3.3, we show the weakest and strongest field ranges inferred from spin equilibrium assuming $\omega_{\rm c} = 0.75$.

3.3.3 Magnetic field inferred from critical luminosity

The presence of a strong magnetic field can increase the critical luminosity of the accreting pulsar by reducing the scattering cross section of photons from electrons [62, 63, 64]. The critical luminosity, $L_{\rm c}$, depends on the magnetic field as $311\,(B/B_{\rm c})^{4/3}\,L_{\rm E}$

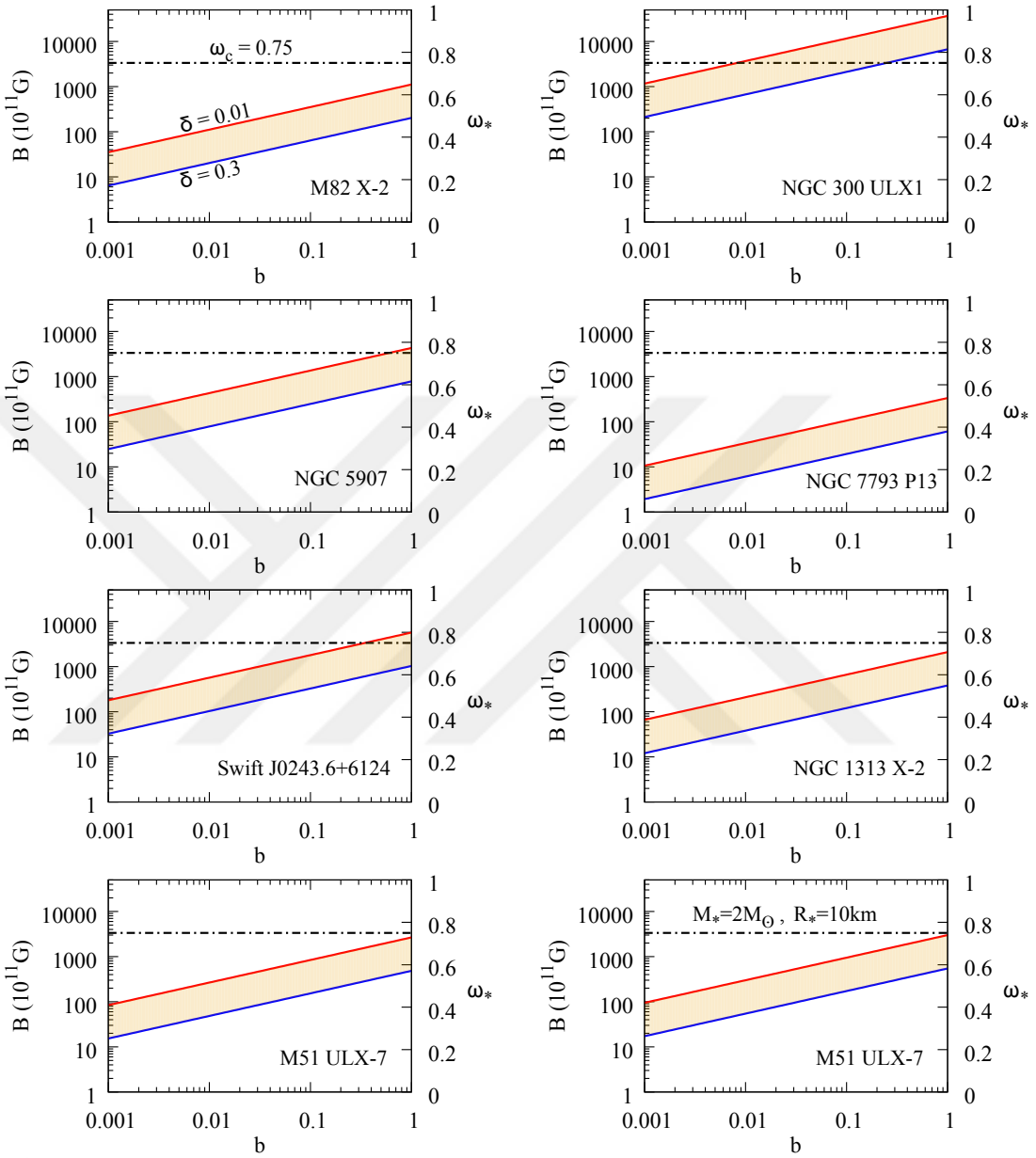

Figure 3.3 : Estimation of the magnetic field (left vertical axis on each panel) and the fastness parameter (right vertical axis on each panel) in terms of the beaming fraction (horizontal axis on each panel), assuming the systems are in spin equilibrium. We use $\omega_c = 0.75$, $\delta = 0.01$ (for red curve), $\delta = 0.3$ (for blue curve) $M_* = 1.4M_\odot$ and $R_* = 10$ km for all sources but to compare two differenet cases for M51 ULX-7 (The bottom-left and-right panels) we use $M_* = 1.4M_\odot$ and $M_* = 2M_\odot$, [74], respectively.

if $L_c \gg L_E$, [63], [80], where $B_c \equiv m_e^2 c^3/\hbar e = 4.4 \times 10^{13}$ G is the quantum critical magnetic field. Magnetic fields above the critical quantum value cause the luminosity to exceed the Edington limit. For sources whose surface magnetic field is well below the critical quantum value, the critical luminosity is almost close to that of Eddington luminosity, $L_c \simeq L_E$.

Critical luminosity is defined as,

$$L_X \leq L_c \simeq \left[1 + 311 \left(\frac{B}{B_c}\right)^{4/3}\right] L_E, \tag{3.24}$$

where $L_X = 4\pi b d^2 F_X$. The surface magnetic field strength for each PULX in terms of the beaming fraction, X-ray flux, and distance is given as

$$B \gtrsim \frac{B_c}{(311)^{3/4}} \left(\frac{4\pi d^2 F_X b}{L_E} - 1\right)^{3/4}. \tag{3.25}$$

The Equation 3.25 yields the minimum magnetic field strength for $L_X = L_c$.

Table 3.4 : Weakest (min) and strongest (max) magnetic field ranges inferred from critical luminosity. For all sources we use $M_* = 1.4 M_\odot$ and $R_* = 10$ km.

Source	$B_{min}(\times 10^9 \mathrm{G})$	$B_{max}(\times 10^{13} \mathrm{G})$
ULX NGC 5907	$0.40 - 2.3$	9.0
ULX NGC 7793 P13	$0.40 - 2.2$	$0.45 - 1.2$
M82 X-2 (J095551+6940.8)	$0.40 - 2.2$	0.85
NGC 300 ULX1	$0.40 - 2.2$	0.67
M51 ULX-7	$0.40 - 2.3$	0.92
NGC 1313 X-2	$0.40 - 2.2$	2.0
Swift J0243.6+6124	$0.40 - 2.2$	0.30

In Figure 3.4, when the X-ray luminosity is equal to the critical luminosity, the minimum values of B and the corresponding fastness parameter values are obtained. The upper limit of the beaming fraction $(b = 1)$ defines the largest value of the minimum magnetic field for $(\omega_* < 1)$. For each PULX, except ULX NGC 7793 P13, the value of $b = 1$, $(0.01 < \delta < 0.3)$, gives the largest value of the minimum magnetic field. However, for ULX NGC 7793 P13, the upper limit is defined for values of

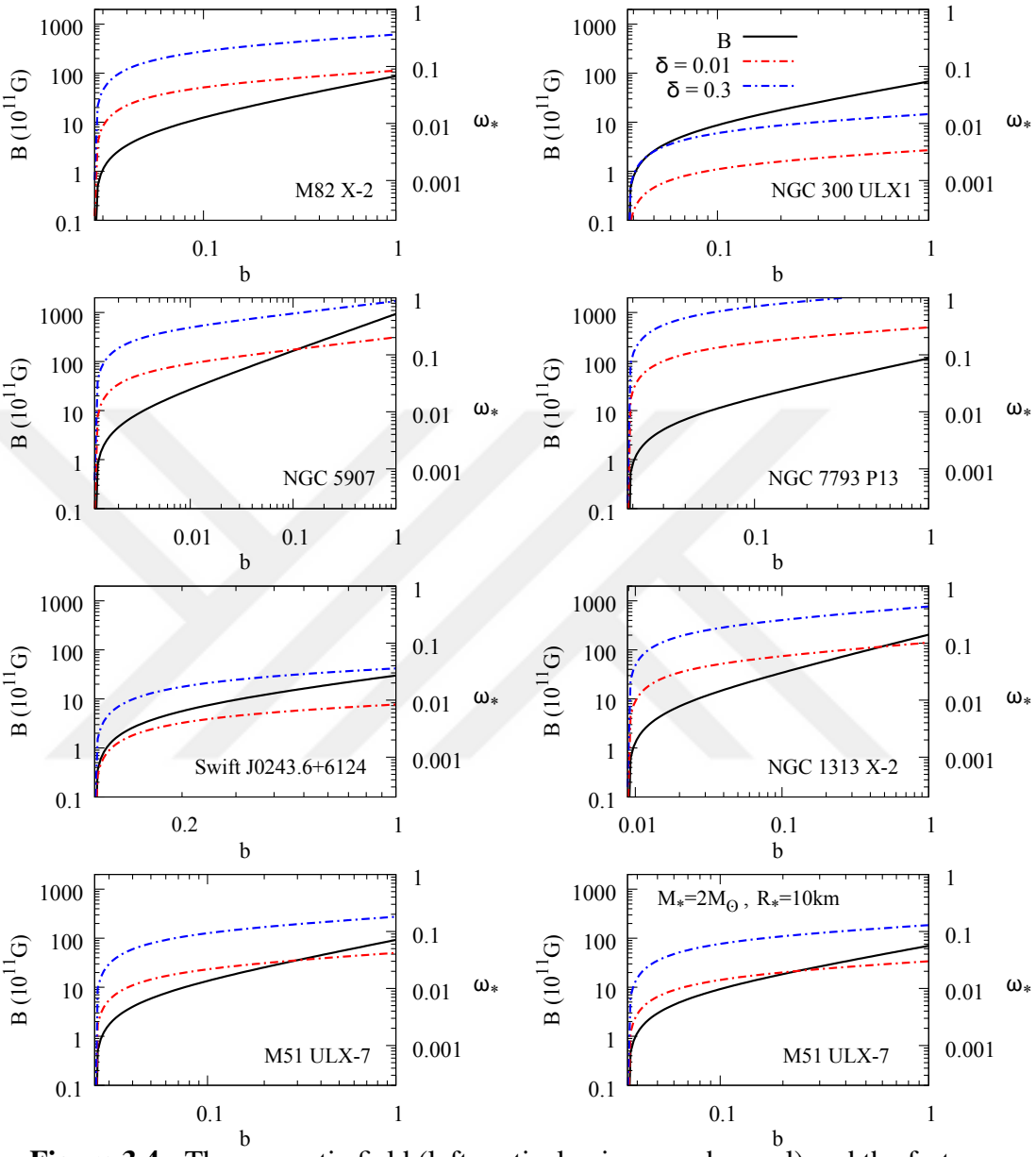

Figure 3.4 : The magnetic field (left vertical axis on each panel) and the fastness parameter (right vertical axis on each panel), in terms of beaming fraction (horizontal axis on each panel), under the assumption of the $L_{\rm X} = L_{\rm c}$. The black solid curves show the magnetic field. We use $\delta = 0.01$ (for red curve), $\delta = 0.3$ (for blue curve) $M_* = 1.4 M_\odot$ and $R_* = 10$ km for all sources but to compare two differenet cases for M51 ULX-7 (The bottom-left and-right panels) we use $M_* = 1.4 M_\odot$ and $M_* = 2 M_\odot$, respectively, [74].

$b < 0.3$, ($\delta = 0.3$). The minimum value of the minimum magnetic field for this source is defined for the range $0.3 < b < 1$. The minimum value range of the minimum magnetic field for all sources is defined for the lower limits of the beaming fraction for which $\omega_* > (R_*/R_{co})^{3/2}$. Our results for the magnetic field ranges inferred from critical luminosity ($L_X = L_c$) are summarized in Table 3.4. The range for all sources in Table 3.4 are obtained for $M_* = 1.4M_\odot$ and $R_* = 10$ km. For a $M_* = 2M_\odot$ neutron star (M51 ULX-7), lower magnetic field and fastness parameter values were obtained. Because, according to Equation 3.25, minimum B values decrease when Eddington luminosity increases.

3.3.4 Common solutions of spin up rate, spin equilibrium and critical luminosity

In this thesis, together with the main methods mentioned above, the value ranges for the magnetic field and fastness parameters are estimated by using the common solutions of these methods with each other.

3.3.4.1 Magnetic field inferred from the spin-up rate and critical luminosity

In this method, we obtained magnetic fields using both spin-up rate and critical luminosity ($L_X = L_c$) assumptions. As can be seen in Figure 3.5 and Figure 3.7, we obtained the magnetic field and fastness parameter values from the intersection of the model curves, based on the observed spin-up ratios and critical luminosity assumptions. Model intersections showed that for each source, similar ranges for both B and ω_* can be obtained. Our model intersects over a wide range of b ($0.01 < \delta < 0.3$) for all sources except NGC 300 ULX1, Swift J0243.6 + 6124, and NGC 1313 X-2 (Figure 3.5, Figure 3.6). For NGC 300 ULX1 source, we obtained marginal solutions for the fastness parameter and the magnetic field around $b = 1$ ($\delta = 0.34$). The value of $\delta = 0.34$ is beyond the upper limit we set in this study. For Swift J0243.6+6124, our model curves only intersect at small mass and radius values. However, we could not get a general solution for the NGC 1313 X-2 source even with mass values as small as $M_* = 0.9M_\odot$.

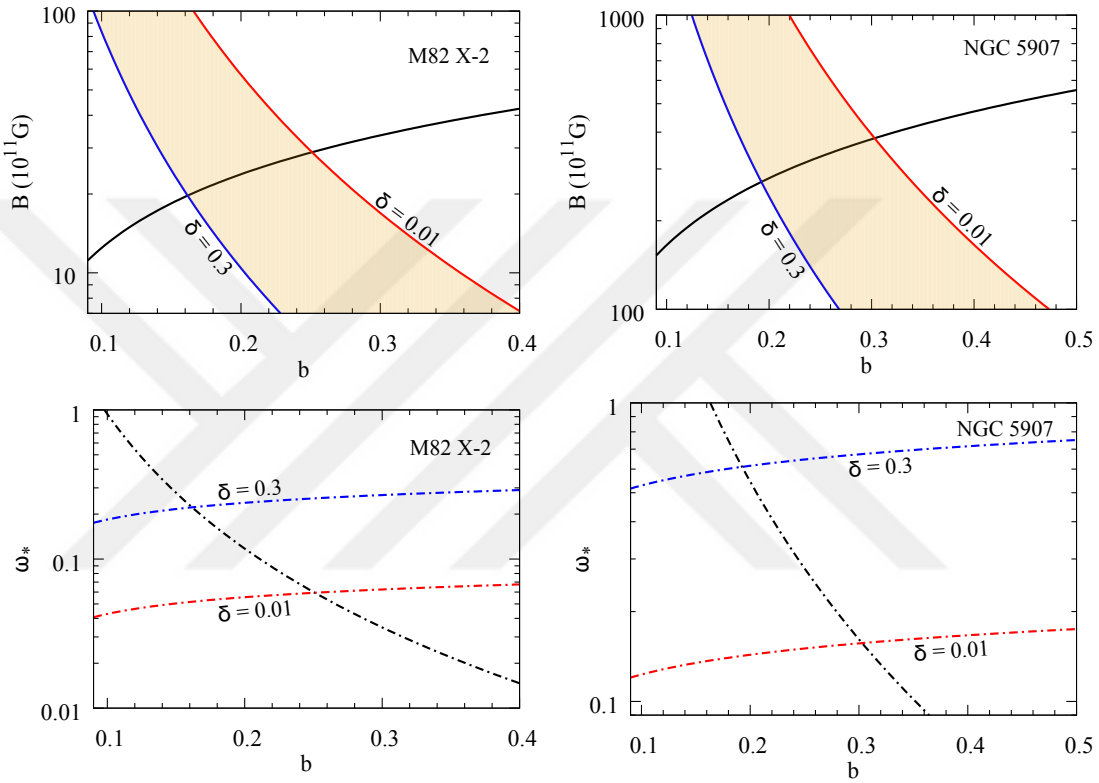

Figure 3.5 : The magnetic field and the fastness parameter in terms of the beaming fraction using the spin-up rates of the PULX M82 X-2 (left panels) and ULX NGC 5907 (right panels) under the assumption of $L_X = L_c$. The solutions for B (vertical axes on the upper panels), b (horizontal axis on each panel) and ω_* (vertical axes on the lower panels) have been achieved by the intersection of black solid curve and red and blue solid curves. We use $M_* = 1.4M_\odot$ and $R_* = 10$ km for each source, [74].

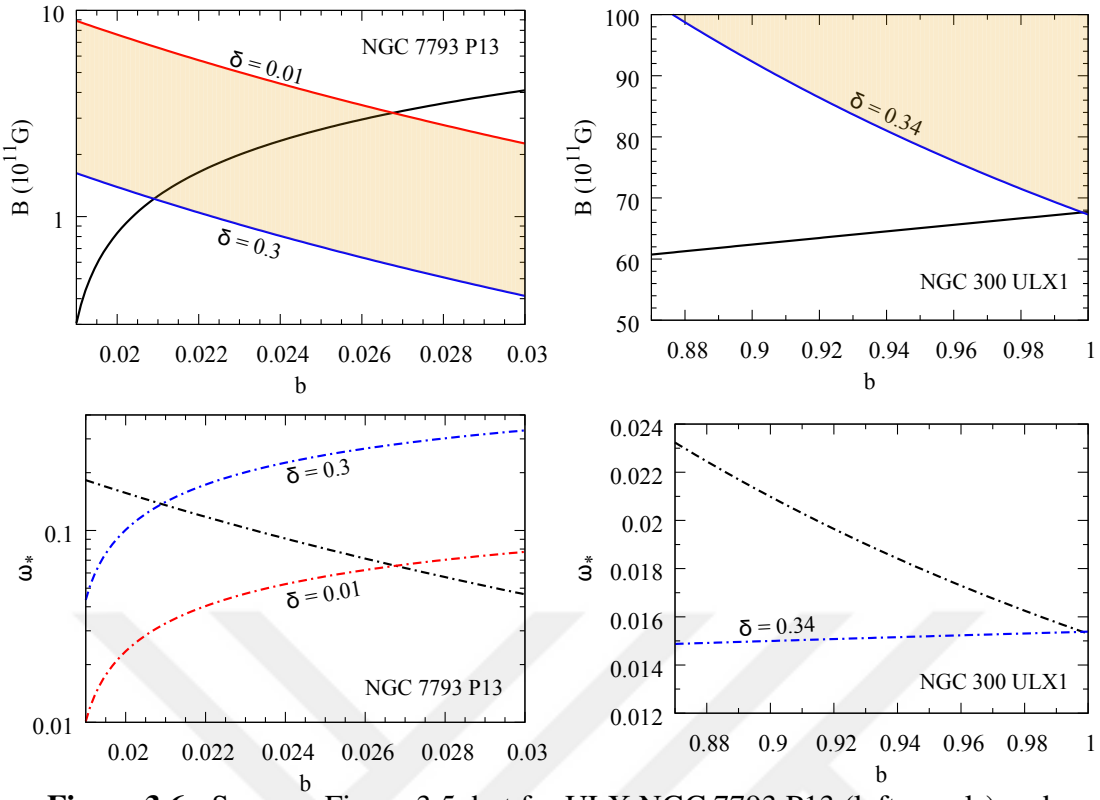

Figure 3.6 : Same as Figure 3.5, but for ULX NGC 7793 P13 (left panels) and NGC 300 ULX1 (right panels). We use $M_* = 1.4M_\odot$ and $R_* = 10$ km for each source.

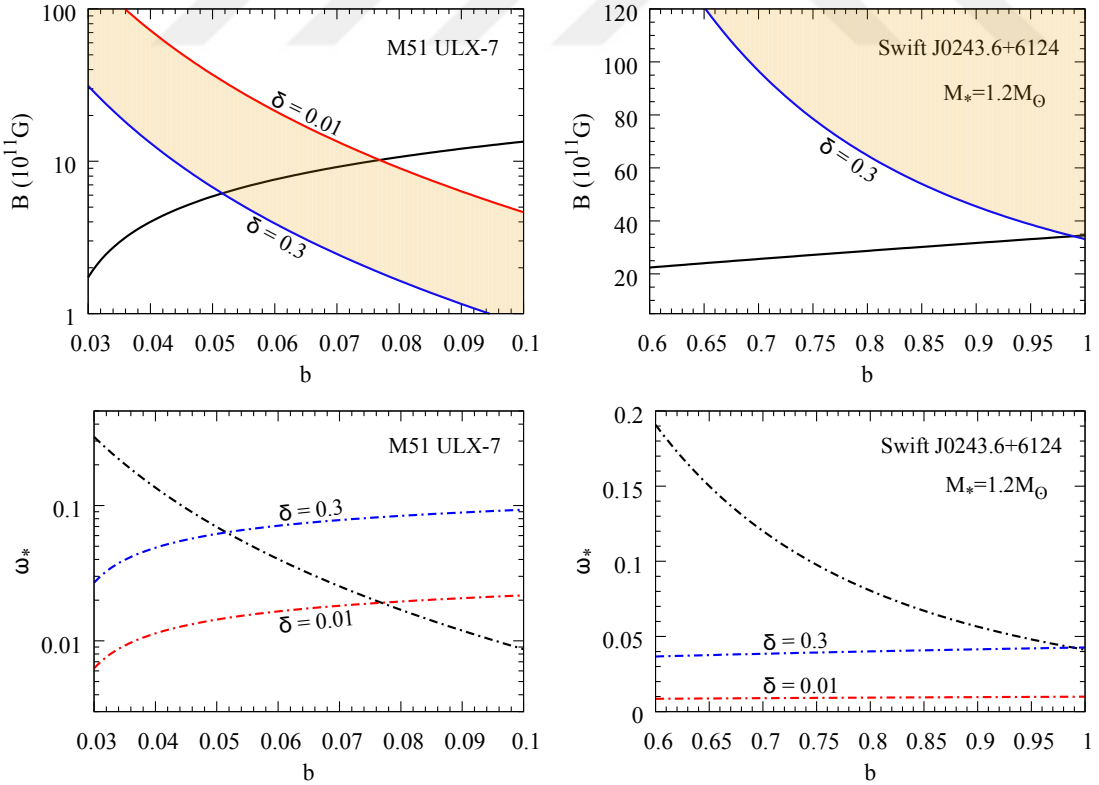

Figure 3.7 : Same as Figure 3.5, but for M51 ULX-7 (left panels) and Swift J0243.6+6124 (right panels). We took $R_* = 10$ km for both sources and $M_* = 1.4M_\odot$ for M51 ULX-7 and $M_* = 1.2M_\odot$ for Swift J0243.6+6124.

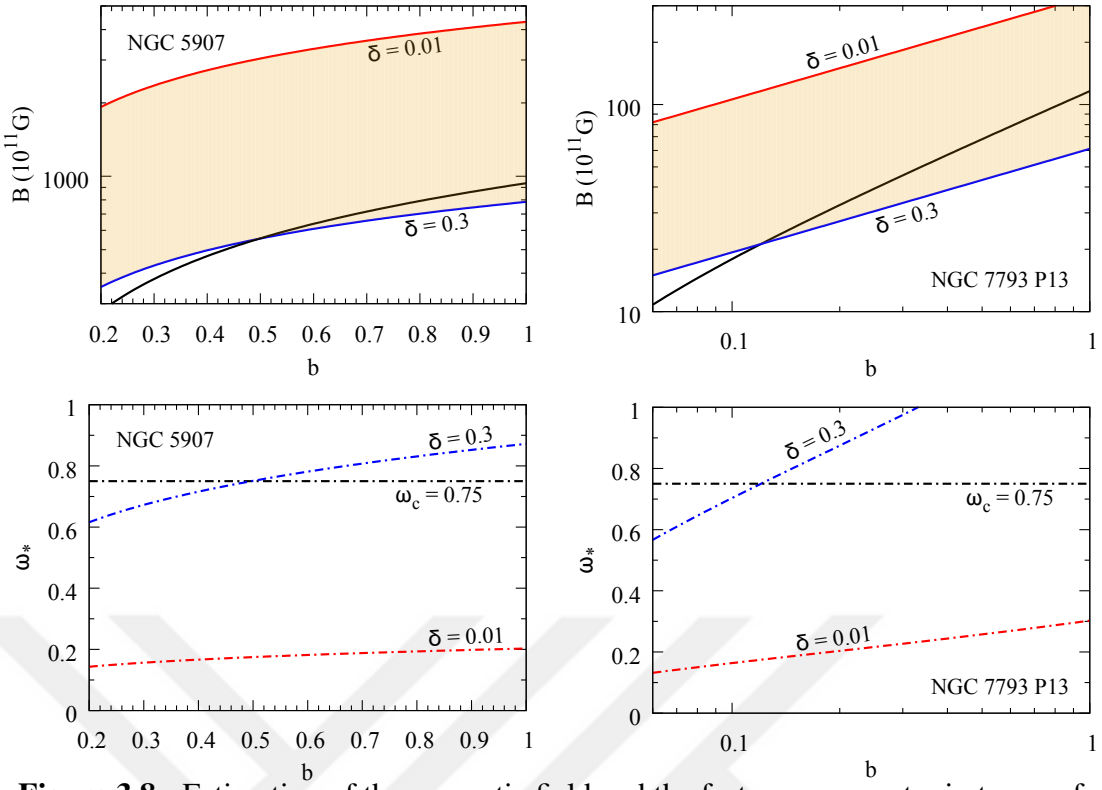

Figure 3.8 : Estimation of the magnetic field and the fastness parameter in terms of the beaming fraction under the ssumption of PULX ULX NGC 5907 (left panels) and ULX NGC 7793 P13 (right panels) are close to spin equilibrium and $L_X = L_c$. The solutions for B (vertical axes on the upper panels), b (horizontal axis on each panel) and ω_* (vertical axes on the lower panels) have been achieved by the intersection of black solid curve and red and blue solid curves. We use $\omega_c = 0.75$, $M_* = 1.4 M_\odot$ and $R_* = 10$ km for each source, [74]

.

3.3.4.2 Magnetic field inferred from the spin equilibrium and critical luminosity

For other PULXs such as M82 X-2, NGC 300 ULX1, M51 ULX-7, NGC 1313 X-2, and Swift J0243.6 + 6124, we could not find a common solution even at extremely small values of neutron star mass. As can be seen in Figure 3.8, relatively large radii and small masses for the neutron stars are required to ensure both spin-equilibrium and critical luminosity conditions.

3.3.4.3 Magnetic field inferred from the subcritical luminosity

The allowed magnetic field region in all PULX with subcritical luminosity is shown in Figure 3.4 above the magnetic field curve depicted by the curve obtained from the critical luminosity assumption. For PULX with subcritical luminosity, the magnetic field results revealed by the subcritical luminosity model obtained under the spin-up

rate and spin equilibrium assumptions are shown in Figure 3.9 and Figure 3.10, respectively.

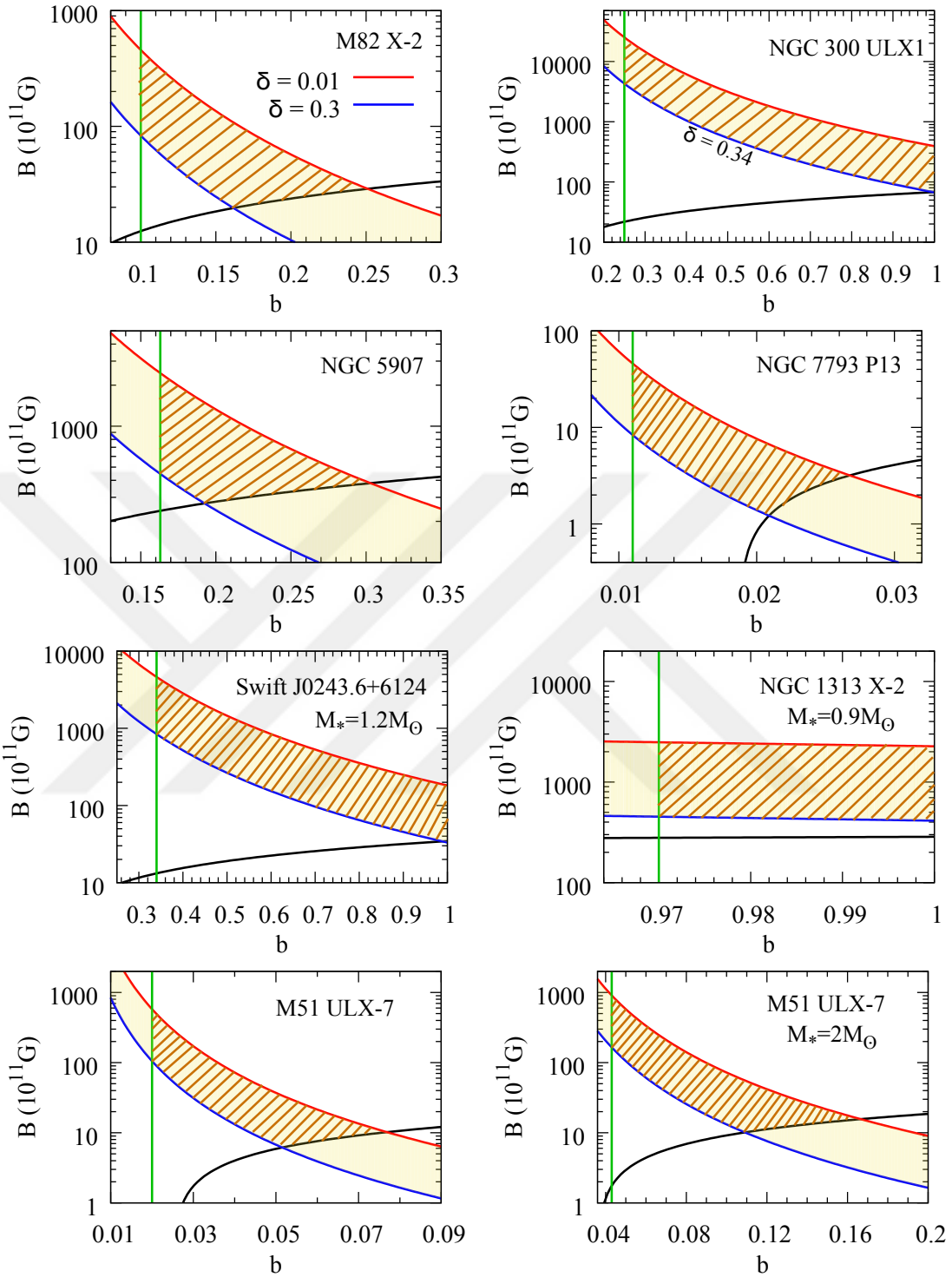

Figure 3.9 : The magnetic field values (shown by striped region) in terms of the beaming fraction using the spin-up rates of PULX at subcritical luminosity. The red and the blue curves show B inferred from spin up rates and the black solid curves show B inferred from critical luminosity. We used $M_* = 1.4M_\odot$ and $R_* = 10$ km for all sources. The bottom-left and -right panels for M51 ULX-7 compare two different cases with $M_* = 1.4M_\odot$ and $M_* = 2M_\odot$, respectively, [74]

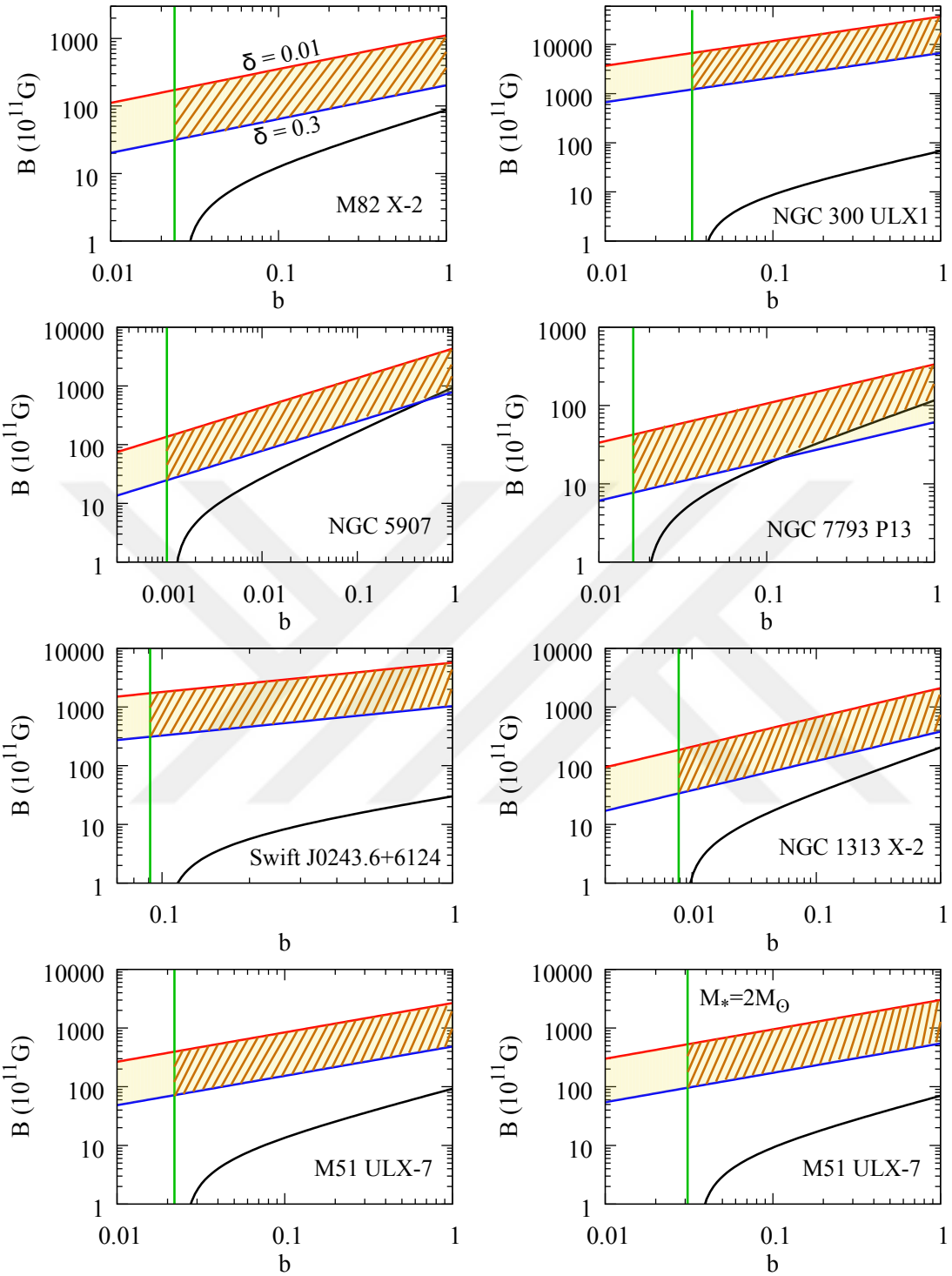

Figure 3.10 : The magnetic field values (shown by striped region) in terms of the beaming fraction using the spin equilibrium of PULX at subcritical luminosity. The red and the blue curves show B inferred from spin equilibrium and the black solid curves show B inferred from critical luminosity. We used $M_* = 1.4M_\odot$ and $R_* = 10$ km for all sources. The bottom-left and -right panels for M51 ULX-7 compare two different cases with $M_* = 1.4M_\odot$ and $M_* = 2M_\odot$, respectively, [74]

.

3.4 Conclusions

In this thesis, we focused on determining the magnetic field, beaming fraction and fastness parameters of PULX. Firstly, we used three different cases for determinig the magnetic fields B, the beaming fraction b, and the fastness parameter ω_* of PULX;

i-) assuming the systems to be in nearly torque equilibrium.

ii-) using the spin up rate and solving torque equation.

iii-) assuming the systems to be accreting at critical rate.

We also examined the systems containing PULX using our methods below;

i-) the observed spin-up rates result from the standard spin-up torque under the critical luminosity condition,

ii-) the spin equilibrium and critical luminosity conditions both apply.

iii-) the subcritical luminosity condition $(L_{\rm X} = L_{\rm c})$ with either the observed spin-up rates or the spin-equilibrium condition.

PULX are most likely systems that transfer mass in the state of $\omega_* < 1$. With the help of the observed spin-up rates, the upper limit of the fastness parameter ($\omega_* = 1$) gives the strong magnetic range corresponding to the lower limit of the beaming. In contrast, the upper limit of beaming fraction, $b = 1$, defines the weak magnetic field range. The limit values of the magnetic fields also depend on the thickness of the boundary region ([72]; see also section 3.2). We calculated the weak magnetic field range corresponding to the lower limit value of b in the super Eddington mass transfer rate case ($\dot{M}_0 > \dot{M}_{\rm E}$) with spin equilibrium $\omega_* = \omega_{\rm c} = 0.75$. If we consider only the critical luminosity, the strongest and weakest ranges of the magnetic fields are determined by the lower and upper ranges of the beaming. We obtain more reliable and tighter constraints on the magnetic fields, beaming fractions, and fastness parameters of the PULX using either the observed spin-up rates or the spin-equilibrium condition along with the critical luminosity condition.

In this thesis, we refer to the state of near spin equilibrium keeping $\omega_* = \omega_c = 0.75$ ([79]) and the state of non-equilibrium assuming an efficient standard spin-up torque. Our study is not based on a specific torque model with a certain dependence on the fastness parameter. Instead, we focus on the spin-equilibrium or spin-up state that occurs due to the torque acting on the neutron star. We think that the reason for observing X-ray pulsation in some ULX and not in others is the beaming. Our calculations here suggest that beaming may also play a role in understanding the lack of pulsations from some of the neutron-star ULX. However, Ekşi et al. (2015), [61], stated that the reason why there is no pulsation in such systems is an optically thick medium due to stellar wind (see also [81]).

Also in this study, we introduced a new approach to beaming. Since our definition of beaming depends on mass transfer rate, magnetic field strength and some other physical parameters, it is more reliable especially for systems that show pulsation.

However, strong gravitational effects around the neutron star's surface are absent in our definition of beaming. The mass-accretion rates and luminosities in PULX are so high that the accretion curtain on the magnetospheric surface can behave as an optically thick, therefore relativistic effects may not be detected ([81]). In the case of large enough mass transfer, the height of the accretion column may be comparable to the radius of the neutron star. For that reason, the X-ray flux from the column is dominant over the reflected component coming from the neutron star surface ([82]). If there is an optically thick envelope around the neutron star, the radial distance of the accretion column can be twice the radius of the neutron star. Therefore, we think that strong gravitational effects can be neglected in pulse profiles of PULX. In the presence of super strong magnetic fields, the reduction of the scattering cross section, [62, 63], can affect the X-ray flux [61], (see also [65, 80, 83]). This argument is based on the assumption that the object is close to spin equilibrium, so very strong magnetic fields are really needed to explain the spin-up of the object. If the system is in outburst state and therefore not in spin equilibrium, the observed spin up rate does not require supercritical magnetic fields, so it supports the beaming argument.

The magnetic field range we have determined by the intersection of our fastness parameter and critical luminosity models reveals the minimum magnetic dipole field strength range on the neutron-star surface. The intersection of our spin-up and critical

luminosity assumptions, the minimum B values we obtained, are well above the weak field range where only spin-up rates are derived. On the other hand, in M82 X-2 and NGC 300 ULX1 (Figure 3.4), the ω_* range deducted from the critical luminosity assumption is well below the critical value of the fastness parameter. This indicates that the sources cannot have X-ray luminosity at the maximum critical value when close to spin equilibrium. In addition, we estimate the surface dipole magnetic fields of the sources, beaming parameters and fastness parameters by including both the observed spin-up ratios (Figure 3.5, Figure 3.6, Figure 3.7) and spin equilibrium conditions (Figure 3.8) under the assumptions of subcritical x-ray luminosity as the most general case. When using observed spin up values, the upper limit of the fastness parameter ($\omega_* = 1$) corresponding to the lower limit of b defines the upper limit of B. However, under the assumption of critical luminosity, the upper limit of b defines the lower limits of B and ω_*.

3.4.1 Comparison with observation

We have applied all possible plausible scenarios to all PULX we have examined in the thesis. The sources we have examined are different from each other when some properties such as the orbital period, the type of the donor star and the spin state of the neutron star are considered. The optical spectrum of NGC 7793 P13 indicates the presence of a blue supergiant companion, while its photometric analysis reveals an orbital period of more than 2 months [84, 85, 86]. ULX NGC 7793 P13 exhibits a slow but persistent spin up [75]. NGC 300 ULX1 is another PULX with a supergiant companion. Photospheric absorption lines in the near infrared spectrum of NGC 300 ULX1 showed that the donor star is a red supergiant with an orbital period of 1–2 years, [87]. A long-term constant spin-up rate with a time span of ~ 1 yr is probably due to the small fastness parameter of NGC 300 ULX1 if the system is away from spin equilibrium, [88]. Under our spin-up ratio and subcritical luminosity assumptions, ULX NGC 7793 P13 ($\omega_* \simeq 0.065$) and NGC 300 ULX1 ($\omega_* \simeq 0.015$) can be slow rotators. However, ULX NGC 7793 P13 can be close to spin equilibrium because the source exhibits a slow spin-up of $\sim -10^{-12}\,\mathrm{s\,s^{-1}}$. We conclude that whether the ULX NGC 7793 P13 and NGC 300 ULX-1 sources are close to spin equilibrium or not, their magnetic fields should be in the range

of $B \sim 10^{11}$ G $- 10^{13}$ G and $B \sim 10^{13}$ G $- 10^{15}$ G, respectively. The intermittent pulsations seen on the M82 X-2 and the large variations in spin-up rate accompanying a secular spin down period indicate that the source may be close to spin equilibrium. Using timing, it was concluded that the mass of the companion star in M82 X-2 is in the range of $M_d = (5-20)M_\odot$ and the orbital period is ~ 2.5 days, [89]. Another PULX ULX 5907 with a secular spin up rate and a short orbital period concluded to be ~ 5 days, [51]. Using the spin-up rates at subcritical luminosity, we obtain similar values for the beaming fraction in the $(0.1-0.3)$ range for both sources. The magnetic field we obtained from the spin-up ratio for the ULX NGC 5907 is one order greater than the magnetic field we obtained for M82 X-2, Figure 3.9. If M82 X-2 is close to spin equilibrium and not close to ULX NGC 5907, then the magnetic field range we get for M82 X2 under the spin equilibrium assumption will have values close to the magnetic field range that we get from spin-up ratio for ULX NGC 5907. Taking $b \sim 0.25$ for both PULX, we find $B = (1-5) \times 10^{13}$ G for M82 X-2 (Figure 3.10) and $B = (3-6) \times 10^{13}$ G for ULX NGC 5907 (Figure 3.9). The mass of the companion star M51 ULX-7, one of the most recently discovered sources in M51, was determined to have a lower limit of about $8M_\odot$ and an orbital period of 2.5 days. It has been suggested that the magnetic dipole field on the surface of the neutron star is approximately $B = 10^{12}$ G $- 10^{13}$ G for $0.08 \leq b \leq 0.25$,[54]. Using the spin-up ratio and the critical luminosity condition (Figure 3.7), we obtained the magnetic field and beaming fraction range as $B = (0.6-1) \times 10^{12}$ G and $0.05 \leq b \leq 0.08$, respectively. However, using spin-up rates with subcritical luminosity, larger field range of $B = (0.6-60) \times 10^{12}$ G is found with $0.02 \leq b \leq 0.08$. Also, the magnetic field lies between 7×10^{12} G and 3×10^{14} G for a beaming fraction in the $\sim 0.02^{\smile} - 1$ range if the system is close to spin equilibrium with a subcritical luminosity. Our field values based on a spin-equilibrium assumption are consistent with the field estimates of Vasilopoulos et al (2019), [88].

Although not precisely determined, the existence of a B-type companion star with an orbital period of about 2 days and a mass of $12M_\odot$ has been proposed for another PULX newly discovered in NGC 1313. The frequency derivatives measured during both pulse detection periods show the presence of spin-up rather than spin down. As also suggested by observations, ULX NGC 1313 X-2 might be close to spin equilibrium and might therefore have $B \sim 10^{12}$ G $- 10^{14}$ G with a minimum beaming

fraction of ~ 0.01 (see Figure 3.10). The first galactic PULX has been discovered Be/X-ray binary Swift J0243.6+6124. The system is known as an X-ray transient with a Be-type main-sequence companion star of mass $16M_{\odot}$ and has an orbital period of 28 days. The system is an X-ray transient and can therefore be either close to or away from spin equilibrium. A sudden increase in the mass accretion rate can push the ULX out of spin equilibrium, and the using the spin up rates under the assumption of subcritical luminosity we deduce $B \sim 10^{12}$ G $- 10^{14}$ G, $b > 0.3$, $\omega_{\star} \geq 0.04$. The source may also be close to spin equilibrium with $\omega_{\star} \simeq 0.04$ and $B \sim 10^{13}$ G $- 10^{14}$ G for $\omega_{\star} \geq 0.1$. We found the narrowest ranges for B, b and $\omega_{\star}$ when we used the critical luminosity condition with observed spin-up rates or spin-equilibrium state. Scenario which is based on spin up rates observed at critical luminosity worked well for all PULX giving B in the $\sim 10^{11}$ G $- 10^{13}$ G range. On the other hand, scenario which is based on the spin-equilibrium at the critical luminosity state worked for two PULX that yielded B only in the $\sim 10^{11}$ G $- 10^{13}$ G range. Assuming subcritical luminosities with observed spin-up rates or spin-equilibrium state, we obtained wider ranges for B, b and $\omega_{\star}$. Using both the observed spin up and spin equilibrium conditions in the subcritical luminosity regime, we found B in the range $\sim 10^{11}$ G $- 10^{15}$ G. As a result of our work, we understand that the surface magnetic dipole fields of neutron stars in PULX are not always magnetar strength. In addition, the B ranges we have obtained include values well below the quantum critical limit for magnetic fields. If the luminosity is considered critical, weaker B fields are obtained. Our results suggest that the role of beaming cannot be ignored. Subcritical luminosity can be reached at the $b < 1$ condition even in the absence of magnetar-strength fields, otherwise it will increase the critical luminosity by reducing the scattering cross section.

4. CONCLUSIONS

In this thesis, we developed a torque model for disc-magnetosphere interaction from the spin and flux observations of *4U 1626–67* and compared it with the torque models in the literature. The method we used is only suitable for a few persistent LMXB because very few of these sources have large magnetic field and show torque reversal. However, as the study is concerned with dimensionless functions depending on dimensionless parameters, we expect our torque model would have implications for models in the literature that have quite different functional form around the torque equilibrium. While the torque inferred from the observations, when ω_*/ω_c is plotted versus n/n_0 exhibits a concave-up behavior around the torque equilibrium, models in the literature predict concave-down behavior. We found that the dimensionless torque has a cubic dependence around equilibrium and can be expressed as the superposition of two hyperbolic functions.This difference may be due to the inadequacy of the models in the literature or the fact that some of the assumptions regarding our model have not been tested yet. One of the uncertainties in our model is due to the coefficient ξ, which determines the relationship between the inner radius and the Alfvén radius. It is possible that this coefficient is not constant and changes depending on the fastness parameter. In future studies, the dependence of the ξ coefficient on the fastness parameter will be investigated. Another uncertainty concerns the assumption that X-ray luminosity will grow with the accretion rate. For example, as observed in the *Her X-1*, the disc may be warped and therefore part of the X-ray flux coming to the observer may be blocked. Yet we think the disk in *4U 1626–67* is not warped, as the system shows a fairly smooth torque evolution around torque equilibrium. Another situation where a linear relation between the accretion rate and the luminosity will not be realized is the regime called ADAF, in which the disc is optically thin and geometrically thick. ADAF regime is generally observed in systems containing black holes. It is therefore unclear how the ADAF regime can be adapted to neutron stars. If, as in the ADAF regime, the local accretion rate in the disk is not proportional to the

amount of material transferred to the surface of the neutron star, our assumption will be invalid.

In this thesis, we also found the critical fastness parameter corresponding to the torque equilibrium of the source as $\omega_c = 0.75$ using the BFM and other this value we have obtained is compatible with other studies. We found that, when the fastness parameter falls below $\omega = 0.6$, we see that an unstable regime emerges, and this instability is a regime seen in simulations. We plan to conduct studies to understand the origin of this erratic behavior.

In this thesis, we have also calculated the surface dipole magnetic fields, B, beaming fractions, b and fastness parameters, ω, of ULX systems showing X-ray pulsation in accordance with different scenarios. In our model based on the spin-up rates at the critical luminosity, the value range we obtained for the magnetic field is compatible with all the PULX. However, the magnetic field range we obtained based on the spin-equilibrium at the critical luminosity yielded consistent results for only two PULX. Our results showed that PULX do not necessarily have magnetar strength magnetic fields. Since most of the magnetic field values we have obtained under different scenarios are well below the critical quantum limit.

We calculated the weak magnetic field range corresponding to the lower limit of b in case of super Eddington mass transfer with spin equilibrium $\omega_* = \omega_c = 0.75$. If we consider only the critical luminosity, the strongest and weakest ranges of the magnetic fields are determined by the upper and lower ranges of beaming. Using the observed spin-up rates or the spin-equilibrium state assumptions with the critical luminosity, we achieved more reliable and tighter constraints on the magnetic fields, the beaming fractions and the fastness parameters of PULX. Our work is not based on a specific torque model with a certain fastness parameter. Instead, we focus on the spin-equilibrium or spin-up state caused by the torque acting on the neutron star. Our calculations here show that beaming may also play a role in understanding the lack of pulsation from some neutron star ULX. Also in this work, we took a new approach to the beaming. Since our definition of the beaming depends on the mass transfer rate, the magnetic field strength and some other physical parameters, it is more reliable especially for pulsating systems. In the presence of super strong magnetic fields, the reduced scattering cross section can affect the X-ray flux. This argument is

based on the assumption that the object is close to spin equilibrium, so really strong magnetic fields are needed to explain the spin-up behavior of the object. If the system is in explosion state and therefore not in spin equilibrium, the observed spin up does not require supercritical magnetic fields, so it supports the beaming argument. The magnetic field range determined by the intersection of our fastness parameter and the critical luminosity models reveals the minimum magnetic dipole field strength range on the neutron-star surface. The intersection of our spin-up and critical luminosity assumptions is that the minimum mgnetic fields we obtained are well above the weak field range from which only spin-up ratios are derived. In addition, we estimate the beaming fraction, the fastness parameters, and the surface dipole magnetic fields of the sources by including both observed the spin-up rates and the spin equilibrium conditions under subcritical x-ray luminosity assumptions as the most general case.

When using observed the spin up values, the upper limit of the fastness parameter corresponding to the lower limit of beaming defines the upper limit of the mgnetic fields. However, under the critical luminosity assumption, the upper limit of the beaming defines the lower limits of magnetic fields and fastness parameter. The scenario based on the spin-up rate worked well for all PULX giving the magnetic fields in the range of 10^{11} G – 10^{13} G. On the other hand, the scenario based on the spin-equilibrium worked for two PULX that yielded magnetic fields in the range of $B \sim 10^{13}$ G – 10^{15} G only. Assuming the subcritical luminosity with observed the spin-up rate or the spin-equilibrium, we obtained larger ranges for the magnetic fields, the beamings and the fastness parameters. Using both the observed spin up and spin equilibrium conditions, we found the subcritical luminosity regime in the range of 10^{11} G – 10^{15} G. As a result of our work, we understand that the surface magnetic dipole fields of the neutron stars in the PULX are not always magnetar strength. In addition, the magnetic field ranges we get include values well below the quantum critical limit for magnetic fields. If the luminosity is considered to be at the critical value, weaker magnetic fields are obtained.

REFERENCES

[1] **Bouvier, J.**, **Alencar, S.H.P.**, **Harries, T.J.**, **Johns-Krull, C.M. and Romanova, M.M.** (2007). Magnetospheric Accretion in Classical T Tauri Stars, *Protostars and Planets V*, 479–494, astro-ph/0603498.

[2] **Warner, B.** (2004). Rapid Oscillations in Cataclysmic Variables, *Publications of the ASP*, *116*, 115–132, astro-ph/0312182.

[3] **Ghosh, P.** (1995). Spin Evolution of Neutron Stars in Binary Systems, *Journal of Astrophysics and Astronomy*, *16*, 289.

[4] **Balbus, S.A. and Hawley, J.F.** (1991). A powerful local shear instability in weakly magnetized disks. I - Linear analysis. II - Nonlinear evolution, *Astrophysical Journal*, *376*, 214–233.

[5] **Shakura, N.I. and Sunyaev, R.A.** (1973). Black holes in binary systems. Observational appearance., *Astronomy and Astrophysics*, *24*, 337–355.

[6] **Url-6<**http://hemel.waarnemen.com/Informatie/Sterren/hoofdstuk6.html#mtr**>**, date retrieved: 10.08.2016.

[7] **Pringle, J.E. and Rees, M.J.** (1972). Accretion Disc Models for Compact X-Ray Sources, *Astronomy and Astrophysics*, *21*, 1.

[8] **Ghosh, P. and Lamb, F.K.** (1979). Accretion by rotating magnetic neutron stars. III - Accretion torques and period changes in pulsating X-ray sources, *Astrophysical Journal*, *234*, 296–316.

[9] **Frank, J.**, **King, A. and Raine, D.J.** (2002). *Accretion Power in Astrophysics: Third Edition*.

[10] **Illarionov, A.F. and Sunyaev, R.A.** (1975). Why the Number of Galactic X-ray Stars Is so Small?, *Astronomy and Astrophysics*, *39*, 185.

[11] **Güngör, C.**, **Ekşi, K.Y.**, **Göğüş, E. and Güver, T.** (2017). Partial Accretion in the Propeller Stage of Low-mass X-Ray Binary Aql X-1, *Astrophysical Journal*, *848*, 13, 1709.02378.

[12] **Spruit, H.C. and Taam, R.E.** (1993). An instability associated with a magnetosphere-disk interaction, *Astrophysical Journal*, *402*, 593–604.

[13] **D'Angelo, C.R. and Spruit, H.C.** (2010). Episodic accretion on to strongly magnetic stars, *Monthly Notices of Royal Astronomical Society*, *406*, 1208–1219, 1001.1742.

[14] **D'Angelo, C.R. and Spruit, H.C.** (2011). Long-term evolution of discs around magnetic stars, *Monthly Notices of Royal Astronomical Society*, *416*, 893–906, 1102.3697.

[15] **D'Angelo, C.R. and Spruit, H.C.** (2012). Accretion discs trapped near corotation, *Monthly Notices of Royal Astronomical Society*, *420*, 416–429, 1108.3833.

[16] **Lovelace, R.V.E.**, **Romanova, M.M. and Bisnovatyi-Kogan, G.S.** (1999). Magnetic Propeller Outflows, *Astrophysical Journal*, *514*, 368–372, astro-ph/9811369.

[17] **Uzdensky, D.A.**, **Königl, A. and Litwin, C.** (2002). Magnetically Linked Star-Disk Systems. II. Effects of Plasma Inertia and Reconnection in the Magnetosphere, *Astrophysical Journal*, *565*, 1205–1215.

[18] **Hayashi, M.R.**, **Shibata, K. and Matsumoto, R.** (1996). X-Ray Flares and Mass Outflows Driven by Magnetic Interaction between a Protostar and Its Surrounding Disk, *Astrophysical Journal Letters*, *468*, L37, astro-ph/9606157.

[19] **Miller, K.A. and Stone, J.M.** (1997). Magnetohydrodynamic Simulations of Stellar Magnetosphere-Accretion Disk Interaction, *Astrophysical Journal*, *489*, 890–902.

[20] **Goodson, A.P.**, **Böhm, K.H. and Winglee, R.M.** (1999). Jets from Accreting Magnetic Young Stellar Objects. I. Comparison of Observations and High-Resolution Simulation Results, *Astrophysical Journal*, *524*, 142–158.

[21] **Romanova, M.M.**, **Ustyugova, G.V.**, **Koldoba, A.V. and Lovelace, R.V.E.** (2009). Launching of conical winds and axial jets from the disc-magnetosphere boundary: axisymmetric and 3D simulations, *Monthly Notices of Royal Astronomical Society*, *399*, 1802–1828, 0907.3394.

[22] **Alpar, M.A. and Shaham, J.** (1985). Is GX5 - 1 a millisecond pulsar?, *Nature*, *316*, 239–241.

[23] **Miller, M.C.**, **Lamb, F.K. and Psaltis, D.** (1998). Sonic-Point Model of Kilohertz Quasi-periodic Brightness Oscillations in Low-Mass X-Ray Binaries, *Astrophysical Journal*, *508*, 791–830, astro-ph/9609157.

[24] **Zhang, C.** (2004). The MHD Alfven wave oscillation model of kHz Quasi Periodic Oscillations of Accreting X-ray binaries, *Astronomy and Astrophysics*, *423*, 401–404, astro-ph/0402028.

[25] **Stella, L. and Vietri, M.** (1998). Lense-Thirring Precession and Quasi-periodic Oscillations in Low-Mass X-Ray Binaries, *Astrophysical Journal Letters*, *492*, L59–L62, astro-ph/9709085.

[26] **Kluźniak, W.**, **Abramowicz, M.A.**, **Kato, S.**, **Lee, W.H. and Stergioulas, N.** (2004). Nonlinear Resonance in the Accretion Disk of a Millisecond Pulsar, *Astrophysical Journal Letters*, *603*, L89–L92, astro-ph/0308035.

[27] **Wang, Y.M.** (1987). Disc accretion by magnetized neutron stars - A reassessment of the torque, *Astronomy and Astrophysics*, *183*, 257–264.

[28] **Matt, S. and Pudritz, R.E.** (2005). Accretion-powered Stellar Winds as a Solution to the Stellar Angular Momentum Problem, *Astrophysical Journal Letters*, *632*, L135–L138, astro-ph/0510060.

[29] **Aly, J.J.** (1980). Electrodynamics of disk accretion onto magnetic neutron star, *Astronomy and Astrophysics*, *86*, 192–197.

[30] **Anzer, U. and Boerner, G.** (1983). Accretion onto rotating, magnetic neutron stars - The inner edge of the disk, *Astronomy and Astrophysics*, *122*, 73–78.

[31] **Aly, J.J. and Kuijpers, J.** (1990). Flaring interactions between accretion disk and neutron star magnetosphere, *Astronomy and Astrophysics*, *227*, 473–482.

[32] **Koenigl, A.** (1991). Disk accretion onto magnetic T Tauri stars, *Astrophysical Journal Letters*, *370*, L39–L43.

[33] **Shu, F.**, **Najita, J.**, **Ostriker, E.**, **Wilkin, F.**, **Ruden, S. and Lizano, S.** (1994). Magnetocentrifugally driven flows from young stars and disks. 1: A generalized model, *Astrophysical Journal*, *429*, 781–796.

[34] **Li, J.**, **Wickramasinghe, D.T. and Ruediger, G.** (1996). Magnetized Accretion and Funnel Flow, *Astrophysical Journal*, *469*, 765.

[35] **Lai, D.** (1998). Transonic Magnetic Slim Accretion Disks and Kilohertz Quasi-periodic Oscillations in Low-Mass X-Ray Binaries, *Astrophysical Journal*, *502*, 721–729, astro-ph/9711142.

[36] **Terquem, C. and Papaloizou, J.C.B.** (2000). The response of an accretion disc to an inclined dipole with application to AA Tau, *Astronomy and Astrophysics*, *360*, 1031–1042, astro-ph/0006113.

[37] **Shirakawa, A. and Lai, D.** (2002). Magnetically Driven Precession of Warped Disks and Millihertz Variabilities in Accreting X-Ray Pulsars, *Astrophysical Journal*, *565*, 1134–1140, astro-ph/0109049.

[38] **Pfeiffer, H.P. and Lai, D.** (2004). Warping and Precession of Accretion Disks around Magnetic Stars: Nonlinear Evolution, *Astrophysical Journal*, *604*, 766–774, astro-ph/0307324.

[39] **Giacconi, R.**, **Murray, S.**, **Gursky, H.**, **Kellogg, E.**, **Schreier, E. and Tananbaum, H.** (1972). The Uhuru catalog of X-ray sources., *Astrophysical Journal*, *178*, 281–308.

[40] **Rappaport, S.**, **Markert, T.**, **Li, F.K.**, **Clark, G.W.**, **Jernigan, J.G. and McClintock, J.E.** (1977). Discovery of a 7.68 second X-ray periodicity in 3U 1626-67, *Astrophysical Journal Letters*, *217*, L29–L33.

[41] **Camero-Arranz, A.**, **Finger, M.H.**, **Ikhsanov, N.R.**, **Wilson-Hodge, C.A. and Beklen, E.** (2010). New Torque Reversal and Spin-up of 4U 1626-67 Observed by Fermi/Gamma-ray Burst Monitor and Swift/Burst Alert Telescope, *Astrophysical Journal*, *708*, 1500–1506, 0906.4224.

[42] **Li, X.D. and Wang, Z.R.** (1996). On the critical "fastness parameter" of a rotating star with a magnetically threaded accretion disk., *Astronomy and Astrophysics*, *307*, L5.

[43] **Colbert, E. and Mushotzky, R.** (1999). The Nature of Accreting Black Holes in Nearby Galaxy Nuclei, *Astrophysical Journal*, *519*, 89–107, astro-ph/9901023.

[44] **Kong, A.**, **Di Stefano, R. and Yuan, F.** (2004). Evidence of an Intermediate-Mass Black Hole: Chandra and XMM-Newton Observations of the Ultraluminous Supersoft X-Ray Source in M101 during Its 2004 Outburst, *Astrophysical Journal Letters*, *617*, L49–L52, astro-ph/0410671.

[45] **Miller, J.**, **Fabian, A. and Miller, M.** (2004). A Comparison of Intermediate-Mass Black Hole Candidate Ultraluminous X-Ray Sources and Stellar-Mass Black Holes, *Astrophysical Journal Letters*, *614*, L117–L120, astro-ph/0406656.

[46] **Liu, J. and Di Stefano, R.** (2008). An Ultraluminous Supersoft X-Ray Source in M81: An Intermediate-Mass Black Hole?, *Astrophysical Journal Letters*, *674*, L73–L76, 0802.0507.

[47] **King, A.**, **Davies, M.**, **Ward, M.**, **Fabbiano, G. and Elvis, M.** (2001). Ultraluminous X-Ray Sources in External Galaxies, *Astrophysical Journal Letters*, *552*, L109–L112, astro-ph/0104333.

[48] **Poutanen, J.**, **Lipunova, G.**, **Fabrika, S.**, **Butkevich, A. and Abolmasov, P.** (2007). Supercritically accreting stellar mass black holes as ultraluminous X-ray sources, *Monthly Notices of Royal Astronomical Society*, *377*, 1187–1194, astro-ph/0609274.

[49] **Gladstone, J.**, **Roberts, T. and Done, C.** (2009). The ultraluminous state, *Monthly Notices of Royal Astronomical Society*, *397*, 1836–1851, 0905.4076.

[50] **Bachetti, M.**, **Harrison, F.**, **Walton, D.**, **Grefenstette, B.**, **Chakrabarty, D.** *et al.* (2014). An Ultraluminous X-ray Source Powered by An Accreting Neutron Star, *Nature*, *514*, 202–204, 1410.3590.

[51] **Israel, G.L.**, **Belfiore, A.**, **Stella, L.**, **Esposito, P.**, **Casella, P.**, **De Luca, A. and ... Wolter, A.** (2017). An accreting pulsar with extreme properties drives an ultraluminous x-ray source in NGC 5907, *Science*, *355*, 817–819, 1609.07375.

[52] **Carpano, S.**, **Haberl, F.**, **Maitra, C. and Vasilopoulos, G.** (2018). Discovery of pulsations from NGC 300 ULX1 and its fast period evolution, *Monthly Notices of Royal Astronomical Society*, *476*, L45–L49, 1802.10341.

[53] **Sathyaprakash, R.**, **Roberts, T.P.**, **Walton, D.J.**, **Fuerst, F.**, **Bachetti, M.**, **Pinto, C. and ... Soria, R.** (2019). The discovery of weak coherent pulsations in the ultraluminous X-ray source NGC 1313 X-2, *Monthly Notices of Royal Astronomical Society*, *488*(1), L35–L40, 1906.00640.

[54] **Rodríguez Castillo, G.A.**, **Israel, G.L.**, **Belfiore, A.**, **Bernardini, F.**, **Esposito, P.**, **Pintore, F. and ... Brightman, M.** (2019). Discovery of a 2.8 s pulsar in a 2 d orbit High-Mass X-ray Binary powering the Ultraluminous X-ray source ULX-7 in M51, *arXiv e-prints*, arXiv:1906.04791, 1906.04791.

[55] **Shao, Y. and Li, X.D.** (2015). A Population of Ultraluminous X-Ray Sources with an Accreting Neutron Star, *Astrophysical Journal*, *802*, 131, 1502.03905.

[56] **Middleton, M.J. and King, A.** (2017a). Predicting ultraluminous X-ray source demographics from geometrical beaming, *Monthly Notices of Royal Astronomical Society*, *470*, L69–L71.

[57] **Middleton, M.J. and King, A.** (2017b). Erratum: Predicting ULX demographics from geometrical beaming, *Monthly Notices of Royal Astronomical Society*, *471*, L71–L71, 1705.06488.

[58] **Pintore, F.**, **Zampieri, L.**, **Stella, L.**, **Wolter, A.**, **Mereghetti, S. and Israel, G.L.** (2017). Pulsator-like Spectra from Ultraluminous X-Ray Sources and the Search for More Ultraluminous Pulsars, *Astrophysical Journal*, *836*, 113, 1701.03595.

[59] **Wiktorowicz, G.**, **Lasota, J.P.**, **Middleton, M. and Belczynski, K.** (2019). The Observed versus Total Population of ULXs, *Astrophysical Journal*, *875*(1), 53, 1811.08998.

[60] **Gnedin, Y.N. and Sunyaev, R.A.** (1973). The Beaming of Radiation from an Accreting Magnetic Neutron Star and the X-ray Pulsars, *Astronomy and Astrophysics*, *25*, 233.

[61] **Eksi, K.Y.**, **Andac, I.C.**, **Cikintoglu, S.**, **Gencali, A.A.**, **Gungor, C. and Oztekin, F.** (2015). The ultraluminous X-ray source NuSTAR J095551+6940.8: a magnetar in a high-mass X-ray binary., *Monthly Notices of Royal Astronomical Society*, *448*, L40–L42, 1410.5205.

[62] **Canuto, V.**, **Lodenquai, J. and Ruderman, M.** (1971). Thomson Scattering in a Strong Magnetic Field, *Phys.Rev.*, *D3*, 2303–2308.

[63] **Paczynski, B.** (1992). GB 790305 as a very strongly magnetized neutron star, *Acta Astronomica*, *42*, 145–153.

[64] **Mushtukov, A.**, **Nagirner, D. and Poutanen, J.** (2016). Compton scattering S matrix and cross section in strong magnetic field, *Physical Review D*, *93*(10), 105003, 1512.06681.

[65] **Dall'Osso, S.**, **Perna, R. and Stella, L.** (2015b). NuSTAR J095551+6940.8: a highly magnetized neutron star with super-Eddington mass accretion, *Monthly Notices of Royal Astronomical Society*, *449*, 2144–2150, 1412.1823.

[66] **Tsygankov, S.S.**, **Mushtukov, A.A.**, **Suleimanov, V.F. and Poutanen, J.** (2016). Propeller effect in action in the ultraluminous accreting magnetar M82 X-2, *Monthly Notices of Royal Astronomical Society*, *457*, 1101–1106, 1507.08288.

[67] **King, A. and Lasota, J.P.** (2019). No magnetars in ULXs, *Monthly Notices of Royal Astronomical Society*, *485*(3), 3588–3594, 1903.03624.

[68] **Kluźniak, W. and Lasota, J.P.** (2015). An ultraluminous nascent millisecond pulsar, *Monthly Notices of Royal Astronomical Society*, *448*, L43–L47, 1411.1005.

[69] **Christodoulou, D.M.**, **Laycock, S.G.T. and Kazanas, D.** (2018). Not an Oxymoron: Some X-ray Binary Pulsars with Enormous Spinup Rates Reveal Weak Magnetic Fields, *Monthly Notices of Royal Astronomical Society*, 1805.06069.

[70] **Brightman, M.**, **Harrison, F.A.**, **Fürst, F.**, **Middleton, M.J.**, **Walton, D.J.**, **Stern, D.**, **Fabian, A.C.**, **Heida, M.**, **Barret, D. and Bachetti, M.** (2018). Magnetic field strength of a neutron-star-powered ultraluminous X-ray source, *Nature Astronomy*, *2*, 312–316, 1803.02376.

[71] **Walton, D.J.**, **Bachetti, M.**, **Fuerst, F.**, **Barret, D.**, **Brightman, M.**, **Fabian, A.C. and ... Webb, N.** (2018). A Potential Cyclotron Resonant Scattering Feature in the ULX Pulsar NGC 300 ULX1 seen by NuSTAR and XMM-Newton, *ArXiv e-prints*, 1803.07571.

[72] **Erkut, M.H.**, **Ekşi, K.Y. and Alpar, M.A.** (2019). Ultra-luminous X-Ray Sources as Super-critical Propellers, *Astrophysical Journal*, *873*(2), 105, 1708.04502.

[73] **Erkut, M.H. and Alpar, M.A.** (2004). On the Rotational Dynamics of Magnetically Threaded Disks around Neutron Stars, *Astrophysical Journal*, *617*, 461–470, astro-ph/0409545.

[74] **Erkut, M.H.**, **Türkoğlu, M.M.**, **Ekşi, K.Y. and Alpar, M.A.** (2020). On the Magnetic Fields, Beaming Fractions, and Fastness Parameters of Pulsating Ultraluminous X-Ray Sources, *Astrophysical Journal*, *899*(2), 97, 2007.08102.

[75] **Fürst, F.**, **Walton, D.J.**, **Harrison, F.A.**, **Stern, D.**, **Barret, D.**, **Brightman, M. and ... Webb, N.** (2016). Discovery of Coherent Pulsations from the Ultraluminous X-Ray Source NGC 7793 P13, *Astrophysical Journal Letters*, *831*, L14, 1609.07129.

[76] **Wilson-Hodge, C.A.**, **Malacaria, C.**, **Jenke, P.A.**, **Jaisawal, G.K.**, **Kerr, M.**, **Wolff, M.T. and NICER Science Team** (2018). NICER and Fermi GBM Observations of the First Galactic Ultraluminous X-Ray Pulsar Swift J0243.6+6124, *Astrophysical Journal*, *863*(1), 9, 1806.10094.

[77] **Erkut, M.H. and Çatmabacak, O.** (2017). Parallel Tracks as Quasi-steady States for the Magnetic Boundary Layers in Neutron-star Low-mass X-Ray Binaries, *Astrophysical Journal*, *849*, 58, 1710.01590.

[78] **Alpar, M.A.**, **Cheng, A.F.**, **Ruderman, M.A. and Shaham, J.** (1982). A new class of radio pulsars, *Nature*, *300*, 728–730.

[79] **Türkoğlu, M.M.**, **Özsükan, G.**, **Erkut, M.H. and Ekşi, K.Y.** (2017). Constraints on the disc-magnetosphere interaction in accreting pulsar 4U 1626-67, *Monthly Notices of Royal Astronomical Society*, *471*, 422–430, 1706.06800.

[80] **Tong, H.** (2015a). An accreting low magnetic field magnetar for the ultraluminous X-ray source in M82, *Research in Astronomy and Astrophysics*, *15*, 517, 1411.3168.

[81] **Mushtukov, A.A.**, **Suleimanov, V.F.**, **Tsygankov, S.S. and Ingram, A.** (2017). Optically thick envelopes around ULXs powered by accreating neutron stars, *Monthly Notices of Royal Astronomical Society*, *467*, 1202–1208, 1612.00964.

[82] **Mushtukov, A.A.**, **Verhagen, P.A.**, **Tsygankov, S.S.**, **van der Klis, M.**, **Lutovinov, A.A. and Larchenkova, T.I.** (2018). On the radiation beaming of bright X-ray pulsars and constraints on neutron star mass-radius relation, *Monthly Notices of Royal Astronomical Society*, *474*(4), 5425–5436, 1707.09822.

[83] **Tong, H.** (2015b). Ultraluminous X-ray pulsar: Accreting magnetar?, *Astronomische Nachrichten*, *336*, 835, 1508.03115.

[84] **Motch, C.**, **Pakull, M.W.**, **Soria, R.**, **Grisé, F. and Pietrzyński, G.** (2014). A mass of less than 15 solar masses for the black hole in an ultraluminous X-ray source, *Nature*, *514*, 198–201, 1410.4250.

[85] **Fabrika, S.**, **Ueda, Y.**, **Vinokurov, A.**, **Sholukhova, O. and Shidatsu, M.** (2015). Supercritical accretion disks in ultraluminous X-ray sources and SS 433, *Nature Physics*, *11*(7), 551–553, 1512.00435.

[86] **Fürst, F.**, **Walton, D.J.**, **Heida, M.**, **Harrison, F.A.**, **Barret, D.**, **Brightman, M. and ... Kretschmar, P.** (2018). A tale of two periods: determination of the orbital ephemeris of the super-Eddington pulsar NGC 7793 P13, *Astronomy and Astrophysics*, *616*, A186, 1805.05336.

[87] **Heida, M.**, **Lau, R.M.**, **Davies, B.**, **Brightman, M.**, **Fürst, F.**, **Grefenstette, B.W. and ... Harrison, F.A.** (2019). Discovery of a Red Supergiant Donor Star in SN2010da/NGC 300 ULX-1, *Astrophysical Journal Letters*, *883*(2), L34, 1909.02171.

[88] **Vasilopoulos, G.**, **Petropoulou, M.**, **Koliopanos, F.**, **Ray, P.S.**, **Bailyn, C.B.**, **Haberl, F. and Gendreau, K.** (2019). NGC 300 ULX1: spin evolution, super-Eddington accretion, and outflows, *Monthly Notices of Royal Astronomical Society*, *488*(4), 5225–5231, 1905.03740.

[89] **Bachetti, M.**, **Maccarone, T.J.**, **Brightman, M.**, **Brumback, M.C.**, **Fürst, F.**, **Harrison, F.A. and ... Walton, D.J.** (2020). All at Once: Transient Pulsations, Spin-down, and a Glitch from the Pulsating Ultraluminous

X-Ray Source M82 X-2, *Astrophysical Journal*, *891*(1), 44, 1905.06423.

APPENDICES

APPENDIX A: Pulse evolution of *4U 1626–67* from 1997 to 2009.

APPENDIX A: Pulse evolution of *4U 1626–67* from 1997 to 2009, [41].

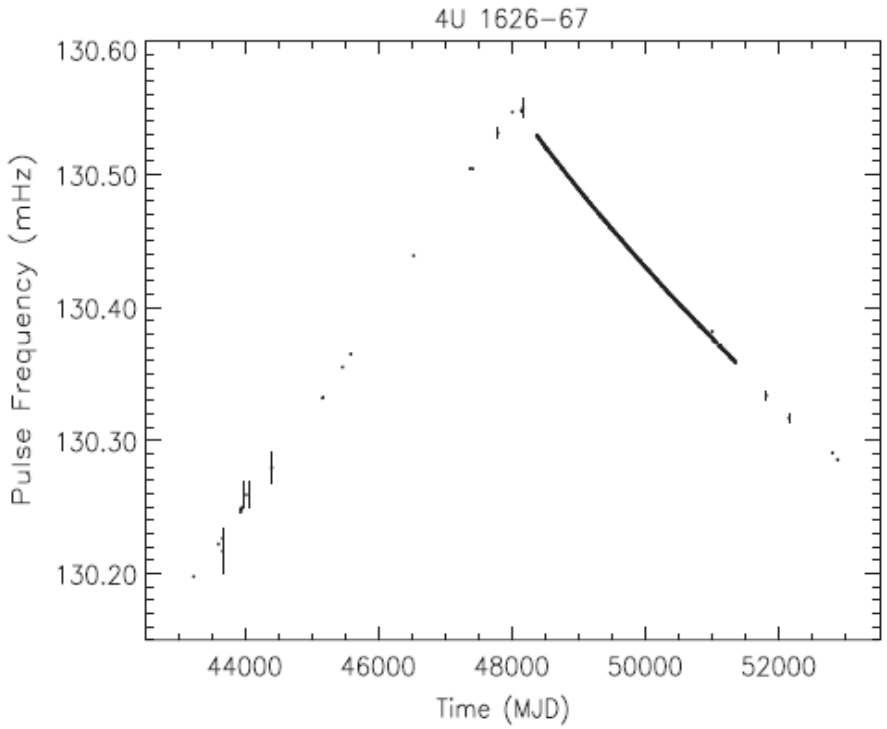

Figure 1 : Pulse evolution of *4U 1626–67*.

CURRICULUM VITAE

Name Surname: Murat Metehan TÜRKOĞLU

B.Sc.: Department of Physics, Science Faculty, Çanakkale Onsekiz Mart University

B.Sc.: Aerospace Engineering, Faculty of Engineering, Middle East Technical University NCC (education continues)

M.Sc.: Mathematical Physics Programme, Astrophysics Research Center and Ulupınar Observatory, Science Faculty, Çanakkale Onsekiz Mart University

PUBLICATIONS/PRESENTATIONS ON THE THESIS

Publications

▪ Constraints on the disc-magnetosphere interaction in accreting pulsar 4U 1626-67. **TÜRKOĞLU, Murat Metehan** ., Özsükan, Gökçe., Erkut, Hakan., Ekşi, K. Yavuz. (2017MNRAS.10.1093/mnras/stx1593)

▪ On the Magnetic Fields, Beaming Fractions, and Fastness Parameters of Pulsating Ultra-luminous X-Ray Sources. Erkut, Hakan., **TÜRKOĞLU, Murat Metehan**., Ekşi, K. Yavuz. 2020APJ.10.3847

Presentations

▪ Poster presentation titled "What does a measurement of mass and/or radius of a neutron star constrain: Equation of state or gravity?" in the meeting: "The 40th COSPAR Scientific Assembly", Moscow, Russia (2014).

OTHER PUBLICATIONS/PRESENTATIONS

Publications

▪ What does a measurement of mass and/or radius of a neutron star constrain: Equation of state or gravity? Ekşi, Kazım Yavuz; Güngör, Can; **Türkoğlu, Murat Metehan**. (2014 PhRvD..89f3003E)

▪ Energy content of the wormholes. Ulu Doğru, M.; **TÜRKOĞLU, Murat Metehan**. (2011MPLA; https://doi.org/10.1142/S0217732311036103)

▪ Conformal cylindrically symmetric space-times in modified gravity. **TÜRKOĞLU, Murat Metehan**; Ulu Doğru, M. (2014MPLA; https://doi.org/10.1142/S0217732315502028)

▪ Moment of inertia of neutron star crust in alternative and modified theories of gravity. Staykov, Kalin.; Ekşi, K. Yavuz; Yazadjiev, Stoytcho S.; **TÜRKOĞLU, Murat Metehan**; Arapoğlu, Savaş. (2016PRD; https://doi.org/10.1103/PhysRevD.94.024056)

Presentations

▪ Oral presentation titled “Energy of Gödel Type wormholes” in the “Turkish Physical Society 27rd International Physics Congress” , Bodrum, Turkey (2009).

▪ Poster presentation titled “Energy of Wrapped Black String” in the “Turkish Physical Society 27rd International Physics Congress” , Bodrum, Turkey (2009).

▪ Poster presentation titled “Energy of 5-D Schwarzschild Black Hole” in the “Turkish Physical Society 27rd International Physics Congress” , Bodrum, Turkey (2009).